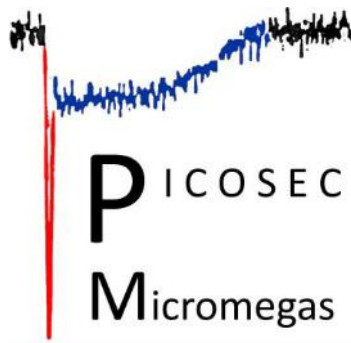# Precise Timing with the PICOSEC Micromegas Detector

Ioannis Manthos

on behalf of the RD51 PICOSEC-Micromegas Collaboration

RD51 PICOSEC-MicroMegas Collaboration

- **CEA Saclay (France):** D. Desforge, I. Giomataris, T. Gustavsson, C. Guyot, F. J. Iguaz[1], M. Kebbiri, P. Legou, O. Maillard, T. Papaevangelou, M. Pomorski, P. Schwemlilg, E. Scorsone, L. Sohl

- **CERN (Switzerland):** J. Bortfeldt, F. Brunbauer, C. David, J. Frachi, M. Lupberger, H. Müller, E. Oliveri, F. Resnati, L. Ropelewski, T. Schneider, P. Thuiner, M. van Stenis, R. Veenhof[2], S. White[3]

- **USTC (China):** J. Liu, B. Qi, X. Wang, Z. Zhang, Y Zhou

- **AUTH (Greece):** K. Kordas, C. Lampoudis, I. Maniatis, I. Manthos, V. Niaouris, K. Paraschou, D. Sampsonidis, S.E. Tzamarias

- **NCSR (Greece):** G. Fanourakis

- **NTUA (Greece):** Y. Tsipolitis

- **LIP (Portugal):** M. Gallinaro

- **HIP (Finland):** F. García

- **IGFAE (Spain):** D. González-Díaz

1) Now at Synchrotron Soleil, 91192 Gif-sur-Yvette, France
2) Also MEPhI & Uludag University.
3) Also University of Virginia.

2

Outline

- **PICOSEC MicroMegas: a detector with precise timing**

  - Single-channel prototype in Laser and Particle beams

- **A well-understood detector**

  - Reproduce observed behavior with detailed simulations and a phenomenological model

- **Towards efficient photocathodes**

  - Estimation of the number of photoelectrons per MIP

- **Towards a robust, large-scale detector**

  - Resistive Micromegas, photocathodes, response of multi-channel PICOSEC prototype

Timing with a few 10's of picosecond

- Needs for Precise timing bring us to the **picosec domain**

- E.g., in the **High Luminosity LHC**, 140-200 "pile-up" proton-proton interactions ("vertices") with happen in the same LHC clock, in close space (Gaussian +- 45mm).

- Using precise timing can separate particles coming from the various vertices.

- (3D) tracking of charged particles is not enough to associate them to the correct vertex . Including precise time offers an extra dimension of separation to achieve this.

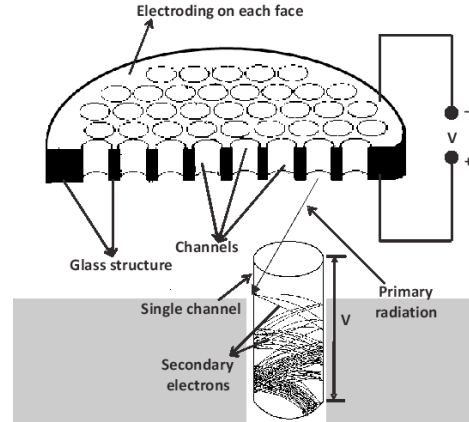- Needed precision: **order ~30ps**
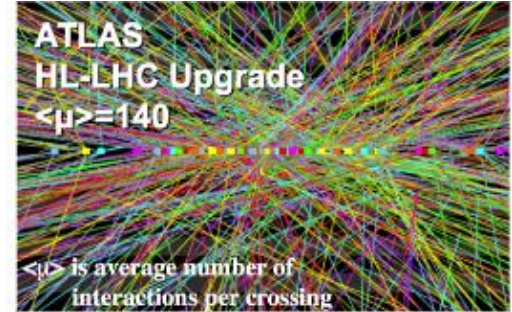
The association of the time measurement to the energy measurement is crucial for physics analysis, and requires time resolution of 20-30ps.
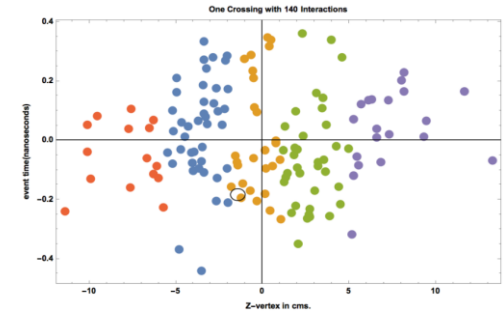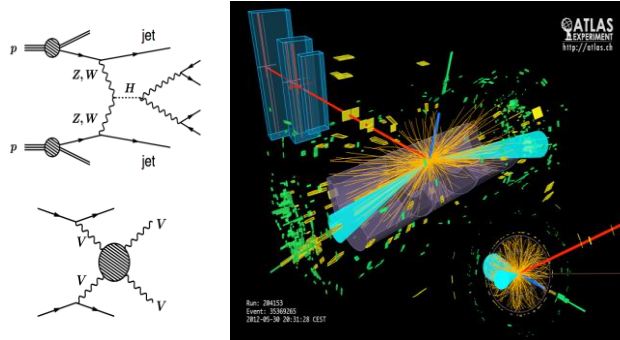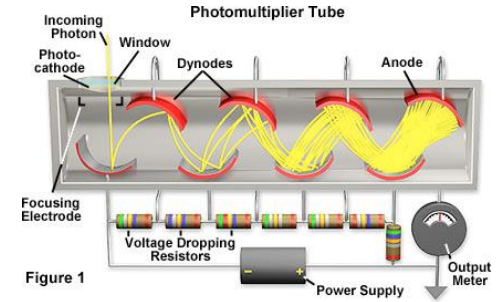
Existing Instrumentation:
e.g. Multi-Channel Plate (MCP) with $\sigma_t \sim 4ps$ but very expensive for large area coverage

PhotoMultiplier: $\sigma_t > 800ps$

Electroding on each face
Channels
Glass structure
Single channel
Secondary electrons
Primary radiation
V

Photomultiplier Tube
Incoming Photon
Window
Photo-cathode
Focusing Electrode
Voltage Dropping Resistors
Dynodes
Anode
Power Supply
Output Meter
Figure 1

Since the hermetic approach at the LHC experiments requires large area coverage, it is natural to investigate both MicroPattern Gas and Silicon structures as candidate detector technologies. However, since the necessary time resolution for pileup mitigation is of the order of 20-30 ps, both technologies require significant modification to reach the desired performance.

Large area detectors, resistant to radiation damage, with ~10ps timing capabilities will find applications in many other domains, e.g.
• particle identification in Nuclear and Particle Physics experiments
• photon's energy/speed measurements and correlations for Cosmology
• optical tracking for charge particles
• 4D tracking in the future accelerators (e.g. FCC with a center energy of ~100TeV)
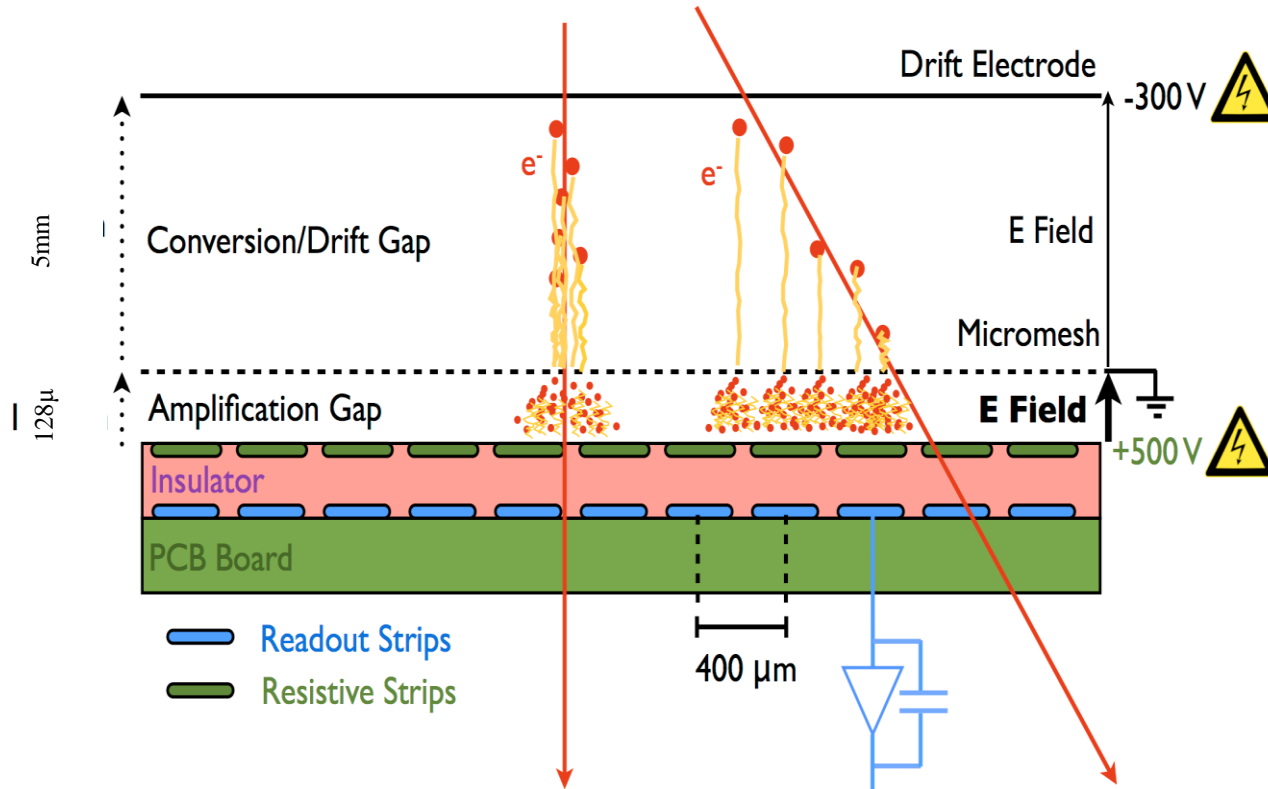
MicroMegas: Micro Pattern Gaseous Chambers

MicroMegas @ ATLAS experiment
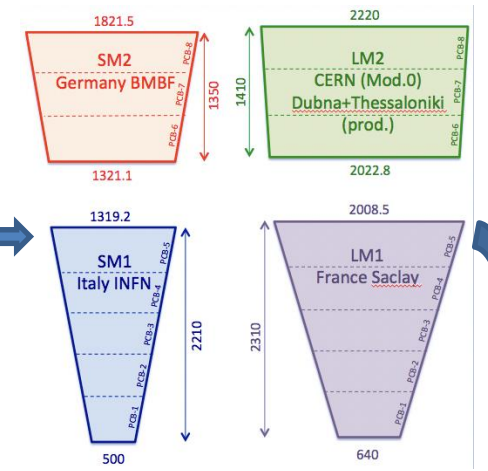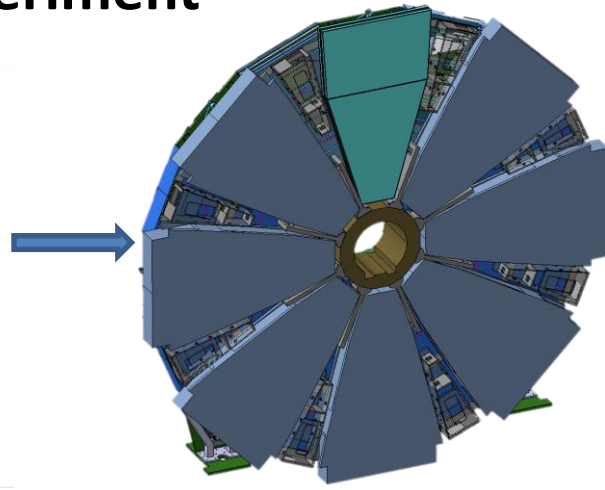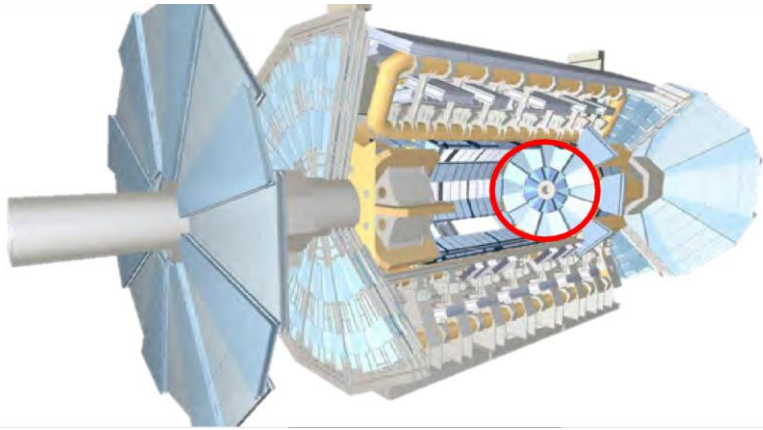
Large area coverage: 1200 m²

- Momentum resolution: better than 15% up to p_t= 1 TeV
- Single plane resolution: 100μm, independent from track angle
- Track segment reconstruction: 50 μm
- Track segment efficiency: >= 97% @ p_t> 10 GeV
- Online angular resolution (trig):   <= 1 mrad
- Spatial resolution 2nd coordinate: ~cm, from stereo strips or wires
- Hit rate capability: 15 kHz/cm² (meeting perform. requ.)
- Accumulated charge without ageing: 1 C/cm² (3000 fb⁻¹ w/o degradation)
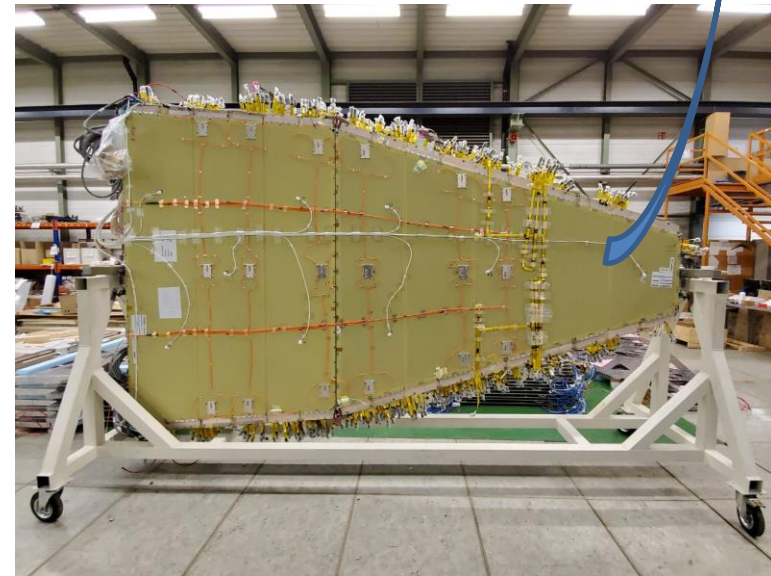
The Physics of Ionization offers the means for precise spatial measurements (high spatial resolution) but inhibits precise timing measurements

10.5170/CERN-1977-009

ORGANISATION EUROPÉENNE POUR LA RECHERCHE NUCLÉAIRE

CERN EUROPEAN ORGANIZATION FOR NUCLEAR RESEARCH

PRINCIPLES OF OPERATION OF MULTIWIRE
PROPORTIONAL AND DRIFT CHAMBERS

F. Sauli

Lectures given in the
Academic Training Programme of CERN
1975-1976

G E N E V A
1977

which is represented in Fig. 8, for n = 34, as a function of the coordinate across a 10 mm thick detector. If the time of detection is the time of arrival of the closest electron at one end of the gap, as is often the case, the statistics of ion-pair production set an obvious limit to the time resolution of the detector. A scale of time is also given in the figure, for a collection velocity of 5 cm/µsec typical of many gases; the FWHM of the distribution is about 5 nsec. There is no hope of improving this time resolution in a gas counter, unless some averaging over the time of arrival of all electrons is realized.

In order to use gaseous detectors for precise (ps) timing of charged particles we should turn other Physics phenomena against the stochastic Nature of ionization

- Cherenkov radiation → provide prompt photons
- Photoelectric effect → convert photons to prompt electrons
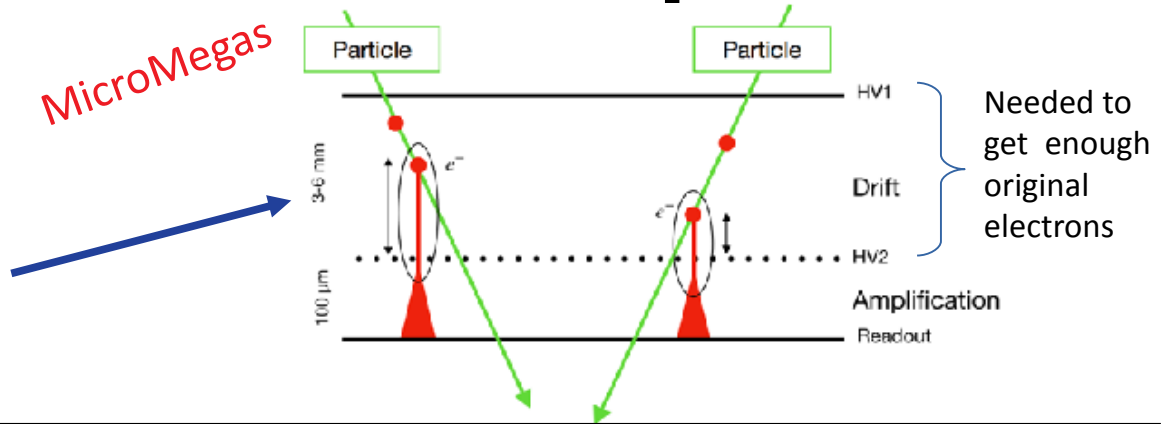
1. A precise-timing detector

Detector concept and the proof
with results of single-channel prototypes

# PICOSEC detector concept

- **Classic Micromegas**

  Giomataris Y. et al., NIMA 376(1996) 29

- Multiple electrons produced at different points along particle's path in the ~3-6mm drift region
  → Time jitter order: **few ns**

Needed to get enough original electrons

- **Micromegas + Cherenkov radiator + photocathode** → synchronous photo-electrons enter Micromegas

- **Small drift gap** & high field → avalanches start as early as possible with minimal time jitter → Timing resolution a **few tens of ps**
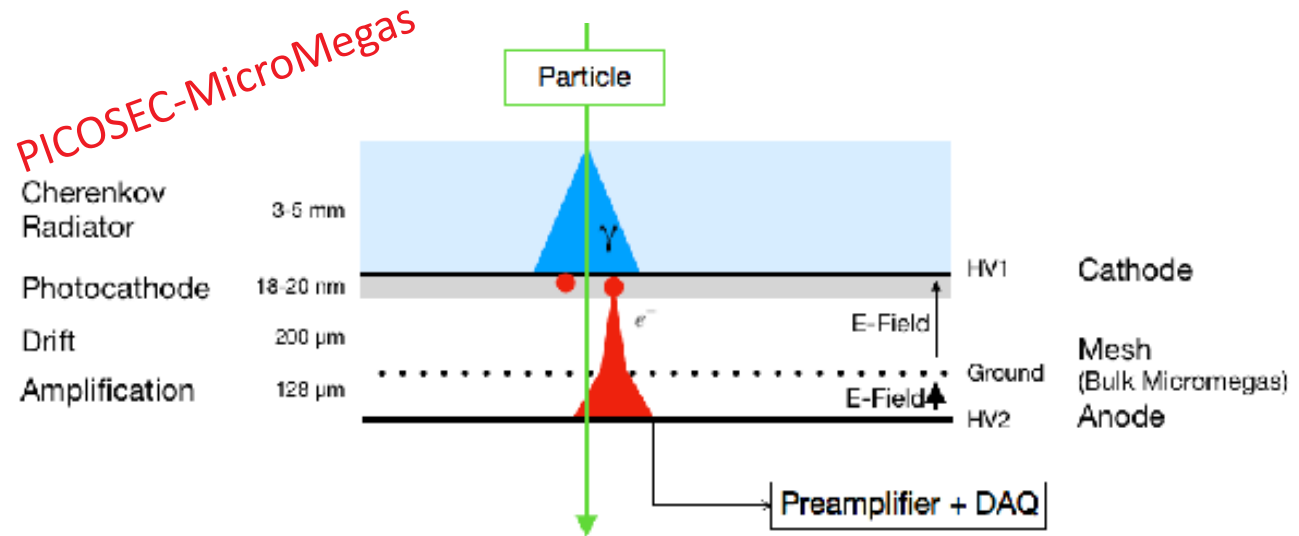
PICOSEC single-channel Prototype

Single pad prototypes - 1 cm diameter active area

1st prototype
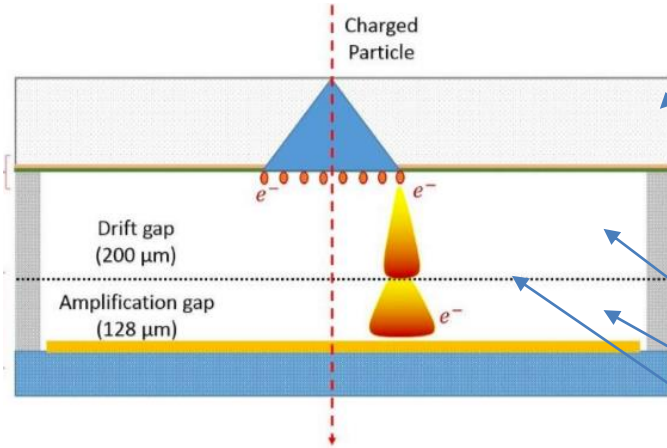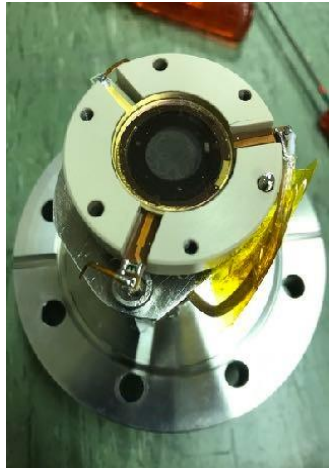
* Cherenkov Radiator:
MgF_2 3 mm thick → <u>3 mm Cherenkov cone</u>

* Photocathode: 18nm CsI (with 5.5 nm Cr - cathode)

* COMPASS gas (80% Ne + 10% CF_4 + 10% C_2H_6)
Pressure: 1 bar.

* Drift gap = 200 μm
* Amplification gap = 128 μm
* Mesh thickness = 36 μm (centered at 128 μm above anode)

- Bulk MicroMegas readout (6 pilars)
- 4 kapton rings spacers → 200 μm drift

Results from Laser and Beam tests presented next are from this detector
Since 2016, different prototypes studied (bulk, thin mesh etc. MM, multipad MM, different gas, anode schemes, photocathodes)

1a.
Response to single photoelectrons

Laser beam: response to single electron (1)

Laser photons

(straight to photocathode)

Cr Layer + CsI

Drift gap   200 µm

Amplification gap   100 µm
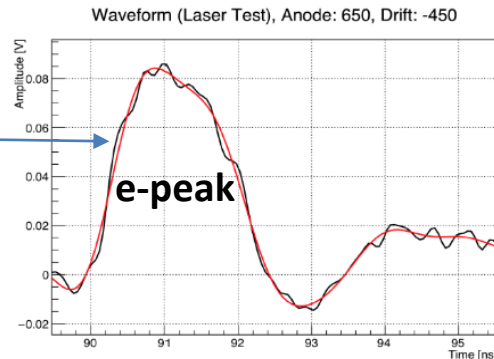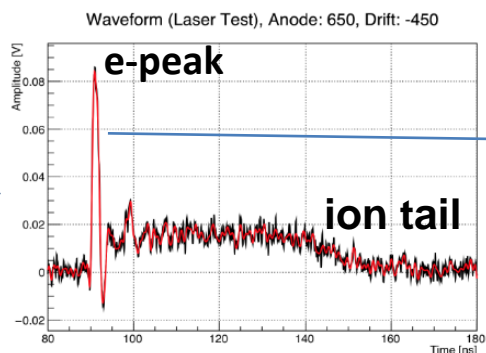
readout

Typical single p.e signal
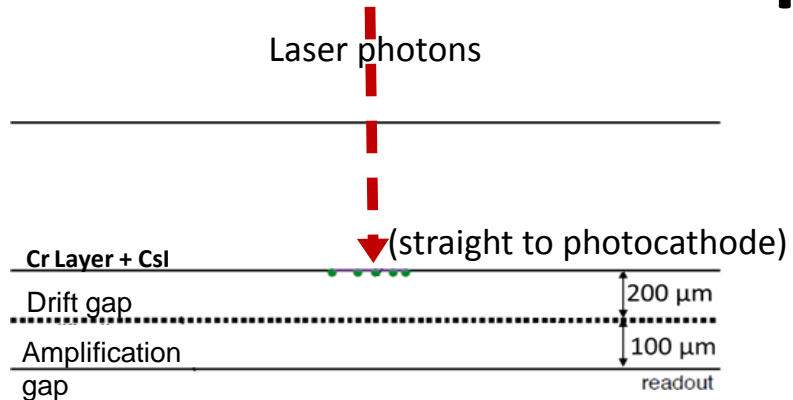
- **Pulsed laser** at IRAMIS facility (CEA Saclay)

- Wavelength: 267-288 nm

- Repetition rate: up to 500 kHz

- **Intensity: attenuated to get single photoelectron directly on photocathode**

- Read out with CIVIDEC preamp

- **Digitized waveform by 2.5GHz LeCroy oscilloscope @ 20GSamples/s = 1 sample/50ps.**

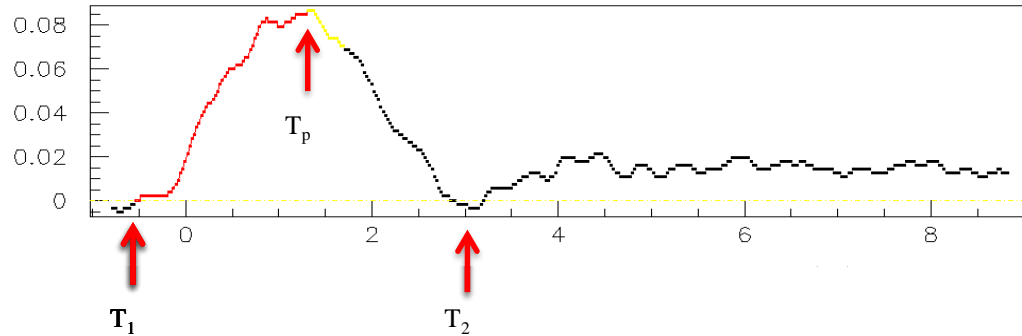- t_0 reference: fast photodiode (~10 ps resolution)
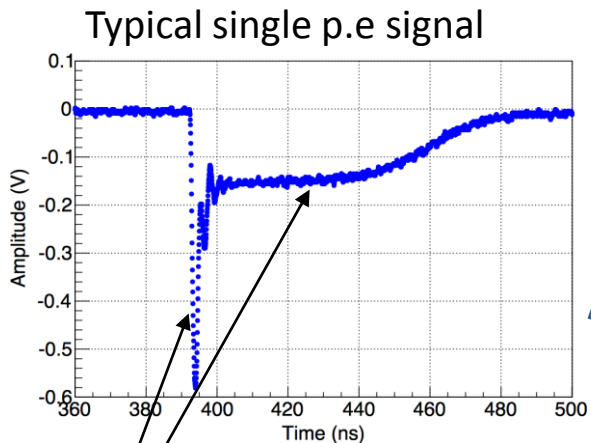
Signal inverted

Two-component signal:
* Electron peak ("*e-peak*") → fast (~0.5ns)
* Ion tail → slow (~100ns)

e-peak

ion tail

e-peak

Waveform (Laser Test), Anode: 650, Drift: -450

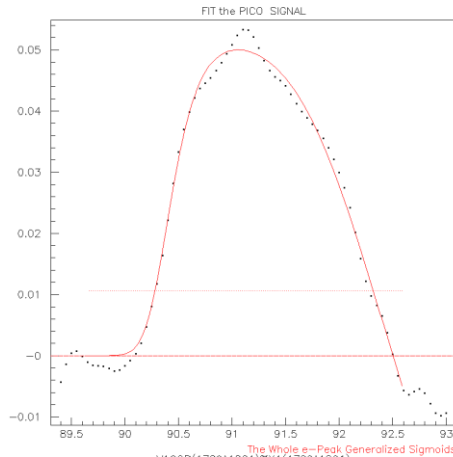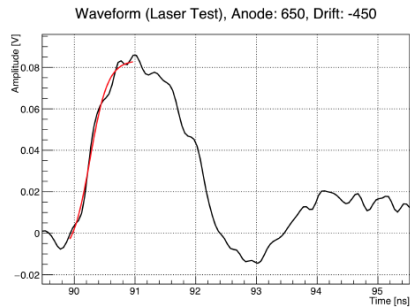Waveform (Laser Test), Anode: 650, Drift: -450

13

Signal processing (1)

- Recognize the "start", "peak" and "end" of the e-peak
- Evaluate charge by integrating the relevant part
- Fit the e-peak pulse in order to neutralize noise effects using the difference of two logistic functions

$$f(t; p_0, p_1, p_2, p_3, p_4, p_5, p_6) = \frac{p_0}{\left(1 + e^{-(t-p_1)p_2}\right)^{p_3}} - \frac{p_0}{\left(1 + e^{-(t-p_4)p_5}\right)^{p_6}}$$


Waveform (Laser Test), Anode: 650, Drift: -450

FIT the PICO SIGNAL

The Whole e—Peak Generalized Sigmoids

The results of these fit are used to define the "**start**" and "**end**" points of the e-peak waveform, to estimate **charge** and it is also used for **timing**
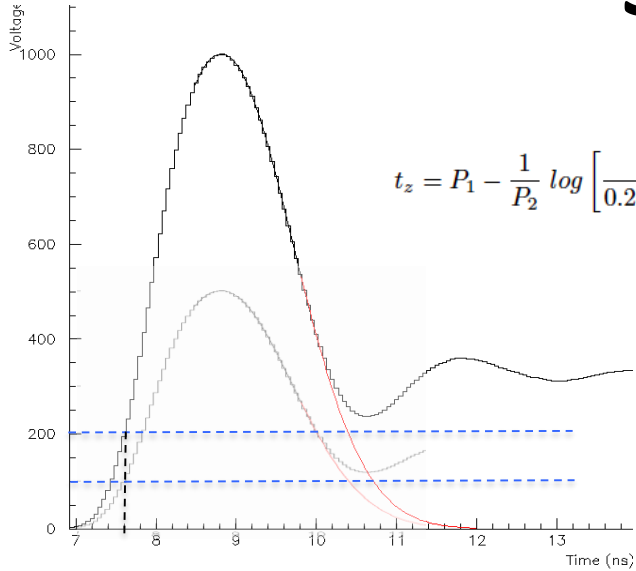
Signal processing (2)

Example: Small pulses
- ✓ Define the start and the end of the e-peak
- ✓ Estimate the charge

**Fitting the e-peak waveform helps to estimate the charge in "impossible" cases**

Single p.e.

Earliest Peak 2 Generalized Logistics
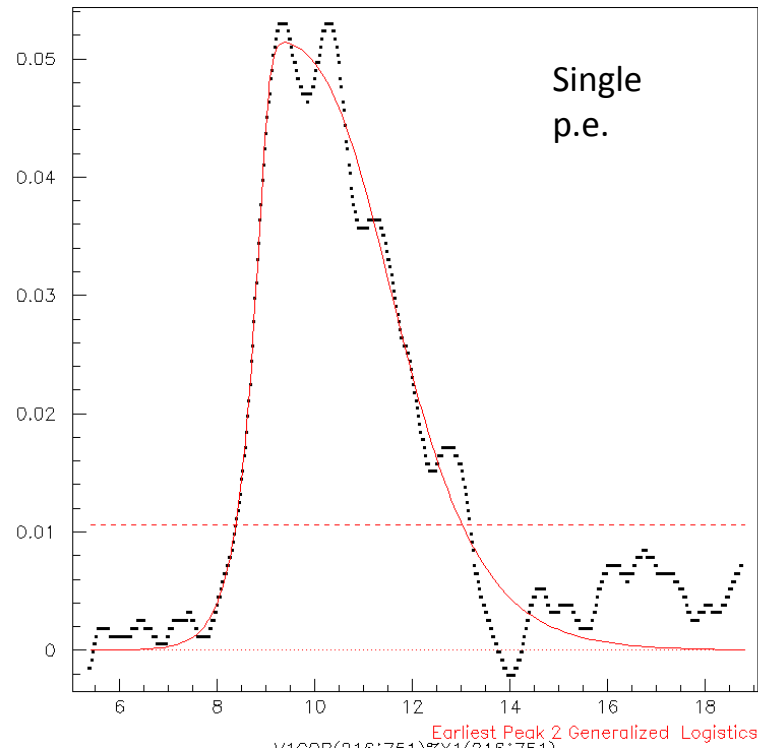
Signal processing (3)

$$t_z = P_1 - \frac{1}{P_2} \log\left[\frac{P_0}{0.2 \times V_{max} - P_3} - 1\right].$$

- Define the e-peak arrival time at a Constant Fraction (CFD) of the peak maximum

- CFD Timing minimizes "slewing effects"

- CFD Timing of raw pulses suffers from noise

- Is it possible to filter-out the noise?

An example of filtering out the noise (cut at 1.5 GHz)
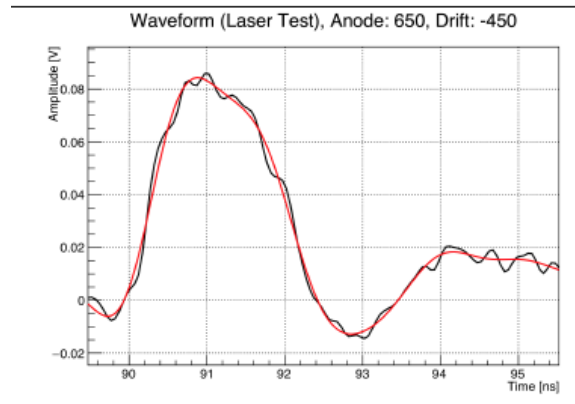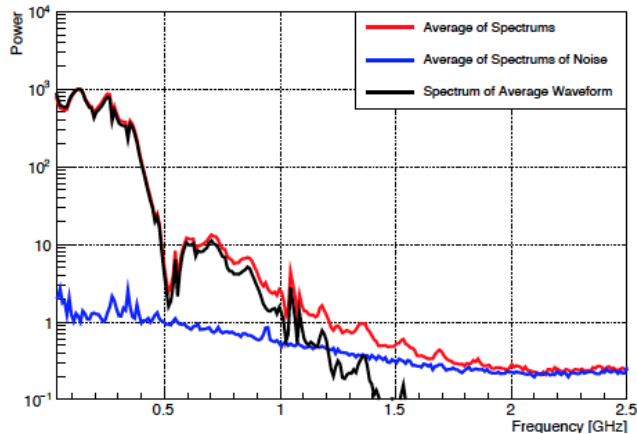
Filtering before fitting the leading edge of the pulse **DOES NOT** improve the timing resolution, i.e. a conservative frequency cut does not improve the timing resolution and a strong frequency cut deforms the rising edge of the pulse worsening the time resolution.

http://ikee.lib.auth.gr/record/294029

16

Laser beam: response to single electron (2)

T_{e-peak} = Signal Arrival Time (SAT)

SAT of a sample of events = $<T_{e-peak}>$

Time Resolution = RMS[T_{e-peak}]

Waveform (Laser Test), Anode: 650, Drift: -450

e-peak

T_{e-peak} — Time (ns)

→ Time the signal arrival with
Constant Fraction Discrimination (CFD)
on the fitted noise-subtracted e-peak

CFD @ 20% of the e-peak amplitude

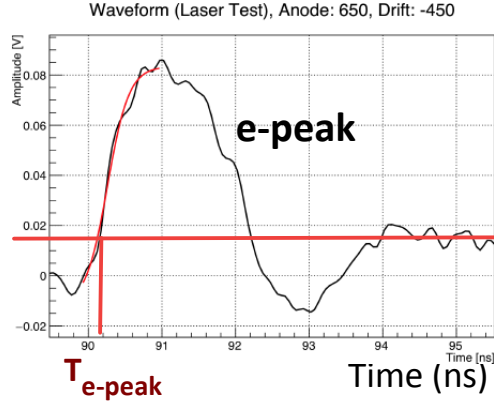- t_0 reference: fast photodiode (~10 ps resolution)

- Detector response at different field settings

- **Timing resolution 76.0 ± 0.4 ps achieved** @ drift/anode: -425V / +450 V

    – improves strongly with higher drift field, less with anode field

Anode 450 V
Anode 475 V
Anode 500 V
Anode 525 V
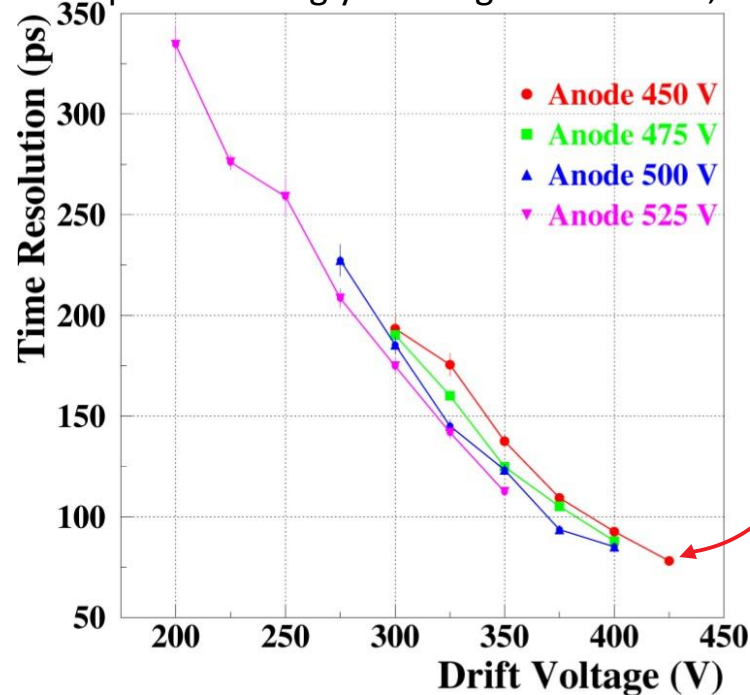
Laser beam: response to single electron (3)

T$_{e\text{-peak}}$ = Signal Arrival Time (SAT)
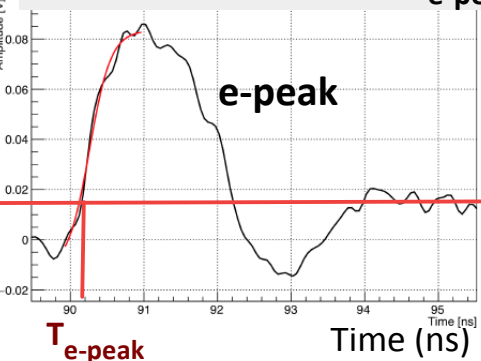
SAT of a sample of events = <T$_{e\text{-peak}}$>

Time Resolution = RMS[T$_{e\text{-peak}}$]

- t$_0$ reference: fast photodiode (~10 ps resolution)

- Detector response at different field settings

- **Timing resolution 76.0 ± 0.4 ps achieved** @ drift/anode: -425V / +450 V

  - improves strongly with higher drift field, less with anode field

  Time Resolution depends mostly on e-peak charge

Waveform (Laser Test), Anode: 650, Drift: -450

e-peak

T$_{e\text{-peak}}$ Time (ns)

Time Resolution (ns) vs Electron Peak Charge (pC)

- Drift 200 V
- Drift 225 V
- Drift 250 V
- Drift 275 V
- Drift 300 V
- Drift 325 V
- Drift 350 V
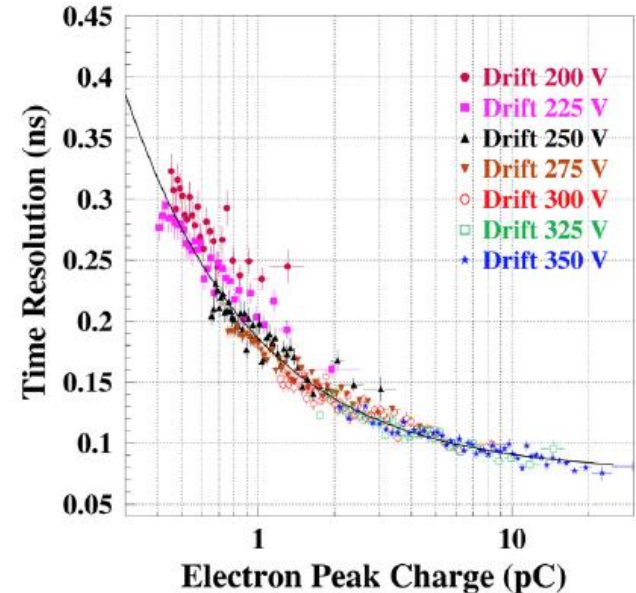
Laser beam: response to single electron (4)

T_{e-peak} = **Signal Arrival Time (SAT)**

SAT of a sample of events = $\langle T_{e-peak} \rangle$

Time Resolution = RMS[T_{e-peak}]

e-peak

T_{e-peak}

Time (ns)
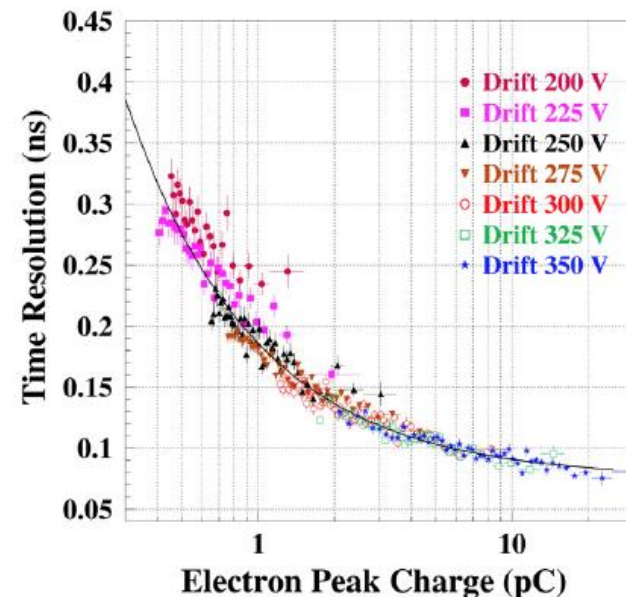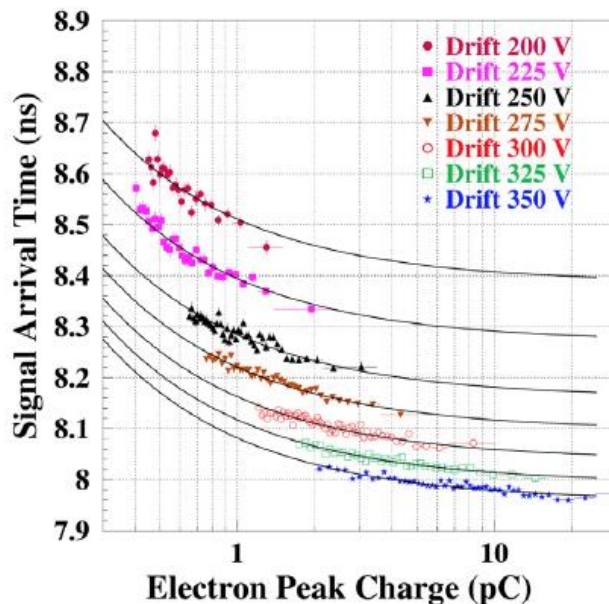
The Signal Arrival Time (SAT) depends non-trivially on the e-peak charge:
- bigger pulses   → smaller SAT
- higher drift field   → smaller SAT

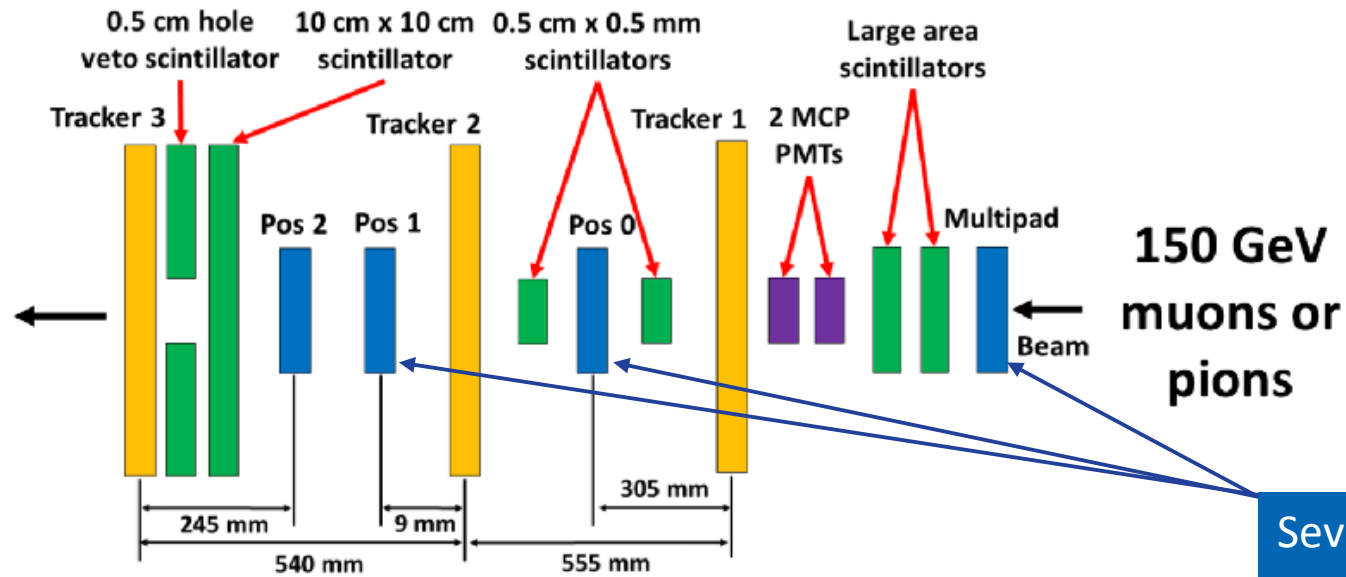* Shape of pulse is identical in all cases → timing with CFD method does not introduce dependence on pulse size
* Responsible for this "slewing" of the SAT: **physics of the detector**

- t_0 reference: fast photodiode (~10 ps resolution)

- Detector response at different field settings

- **Timing resolution 76.0 ± 0.4 ps achieved** @ drift/anode: -425V / +450 V
  - improves strongly with higher drift field, less with anode field

Time Resolution depends mostly on e-peak charge

1b.
Response to Minimum Ionizing Particles (MIPs)

Testing with Particle Beams @ CERN SPS H4

- **Time reference:** two MCP-PMTs (**<5 ps** resolution).
- **Scintillators:** used to select tracks & to avoid showers.
- **Tracking system:** 3 triple-GEMs (**40 μm** precision).
- **Electronics:** CIVIDEC preamp. + 2.5 GHz LeCroy scopes.

Several PICOSEC prototypes tested in parallel

Last run Oct. 2018: The latest for the next 2 years at CERN

Time resolution for MIPs

Red: MCP signal → t_0
Blue: PICOSEC signal
e-peak

$\chi^2 / ndf = 73.26 / 45$
$\mu = 2.7451 + 0.0004$ ns
$\sigma_1 = 20.9 + 0.3$ ps
$\sigma_2 = 38.9 + 1.1$ ps
$\sigma_{Tot} = 24.0 + 0.3$ ps
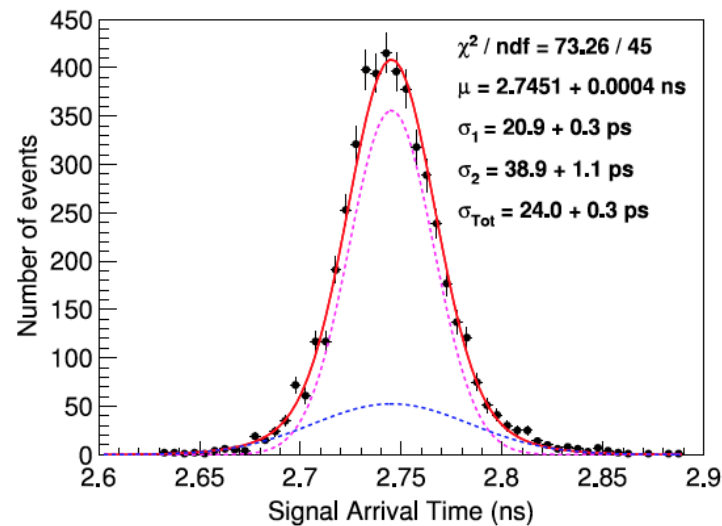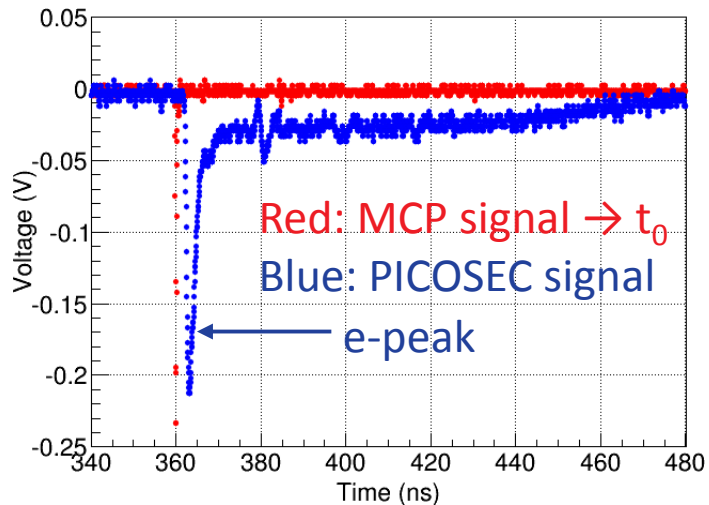
- Same detector as for Laser tests (MgF_2 radiator, CsI photocathode, Bulk MicroMegas, COMPASS gas)

- **Best time resolution: 24ps 24.0±0.3 ps**

- **@ Drift/Anode: -475V/+275V**

"PICOSEC: Charged particle timing at sub-25 picosecond precision with a Micromegas based detector",
J. Bortfeldt et. al. (RD51-PICOSEC collaboration),
Nuclear. Inst. & Methods A 903 (2018) 317-325

Anode = 250 V
Anode = 275 V
Anode = 300 V
Anode = 325 V
Anode = 350 V
Anode = 375 V

22
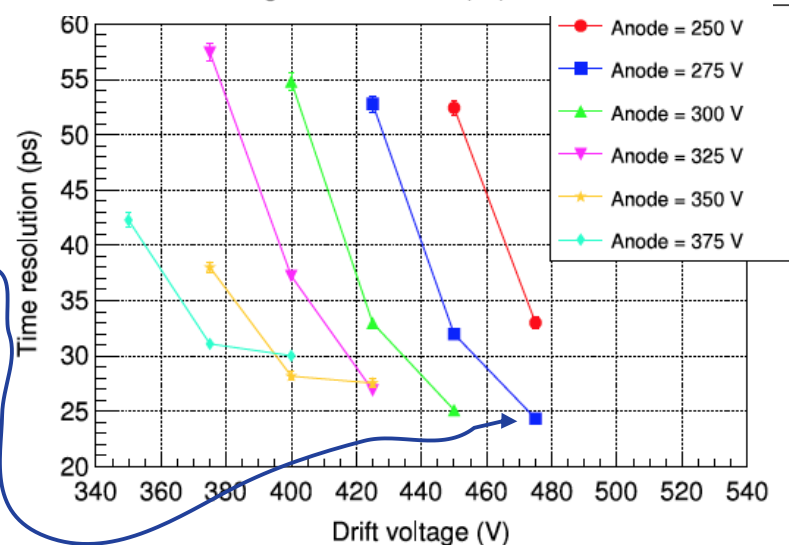
2. A well understood detector

detailed simulations and modeling

Detailed simulation with Garfield++ (1)

Use Garfield++ to simulate PICOSEC for single photoelectrons

ANSYS for the electric field
Anode voltage = 450 V
$\rightarrow$ E = 35 kV/cm
Cathode voltage = 300-425 V
$\rightarrow$ E in [15, 21] kV/cm

Anode voltage does not affect much the timing properties of the signal. So, we split the simulation in three stages:

1) Drift region: simulation till the mesh.

2)Simulation in the amplification region

3) Electronics

Each photoelectron produces $10^5 - 10^6$ other electrons:
A simulation of the amplification region as well would be very time-consuming (~months, to cover the various voltage etc settings tried).

Photo-electron

Cathode

Mesh (Pitch = 63μm, Woven)

Anode

$\Delta z=328\mu m$
$\Delta z=182\mu m$
$\Delta z=200\mu m$
$z=128\mu m$
$\Delta z = 36\ \mu m$
$\Delta z=110\mu m$
$\Delta z=128\mu m$
$z=0\mu m$
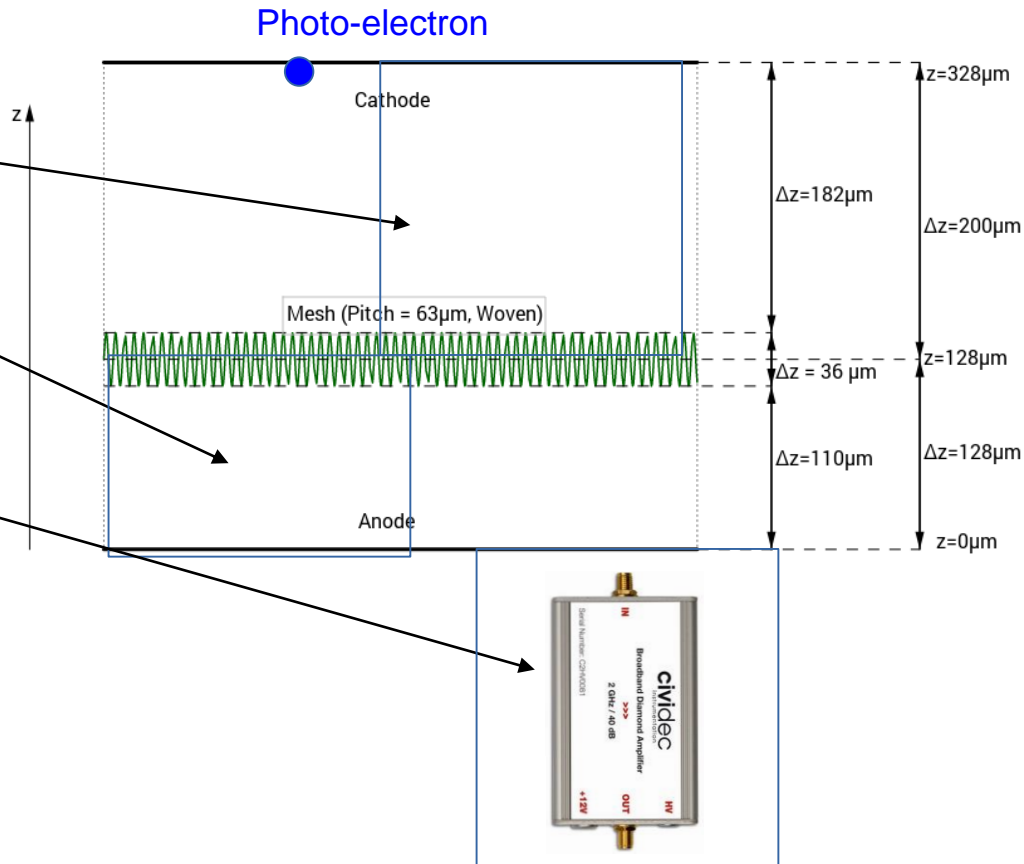
Detailed simulation with Garfield++ (2)

Stage 1 – Drift region

Cathode
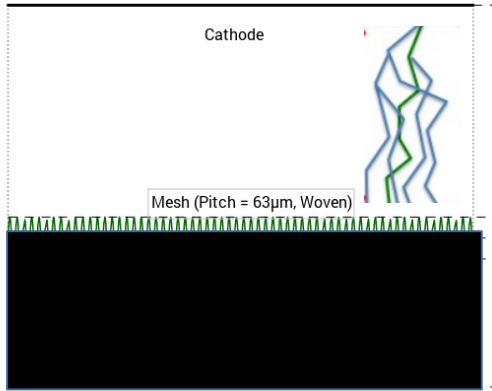
Mesh (Pitch = 63μm, Woven)
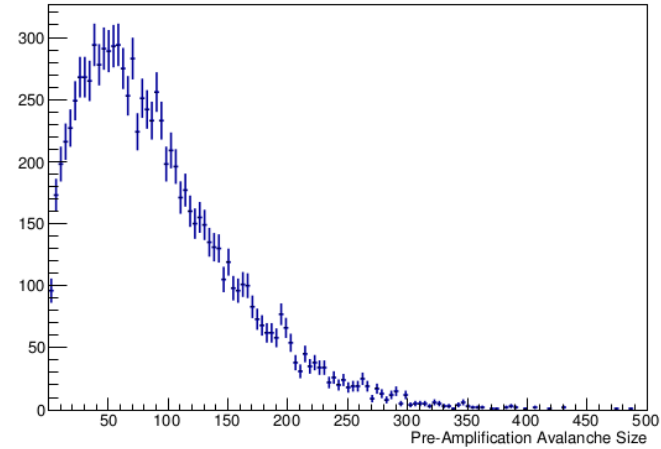
We start with one photoelectron,
and we follow the avalanche it creates
till the mesh.

We then count:
- **how many** electrons pass the mesh and **when**
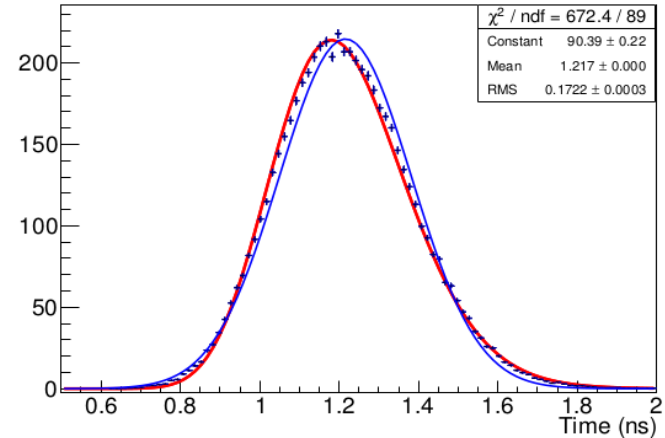
Detailed simulation with Garfield++ (3)

Stage 2 – Amplification Region

Charge = number of electrons

Induced charge

Number of electrons
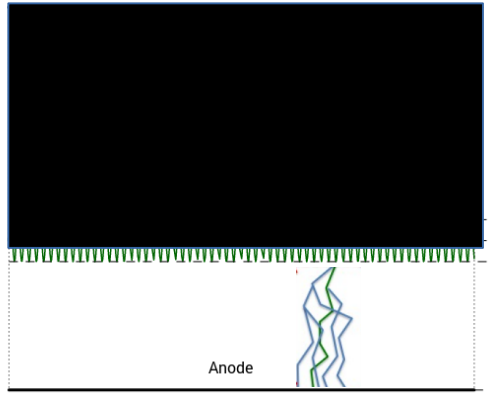
We start from an electron which just passed through the mesh,
we follow the avalanche it produces in the amplification region, and we count **how many electrons** arrive on the anode and the **induced charge**:
one-to-one correspondence.
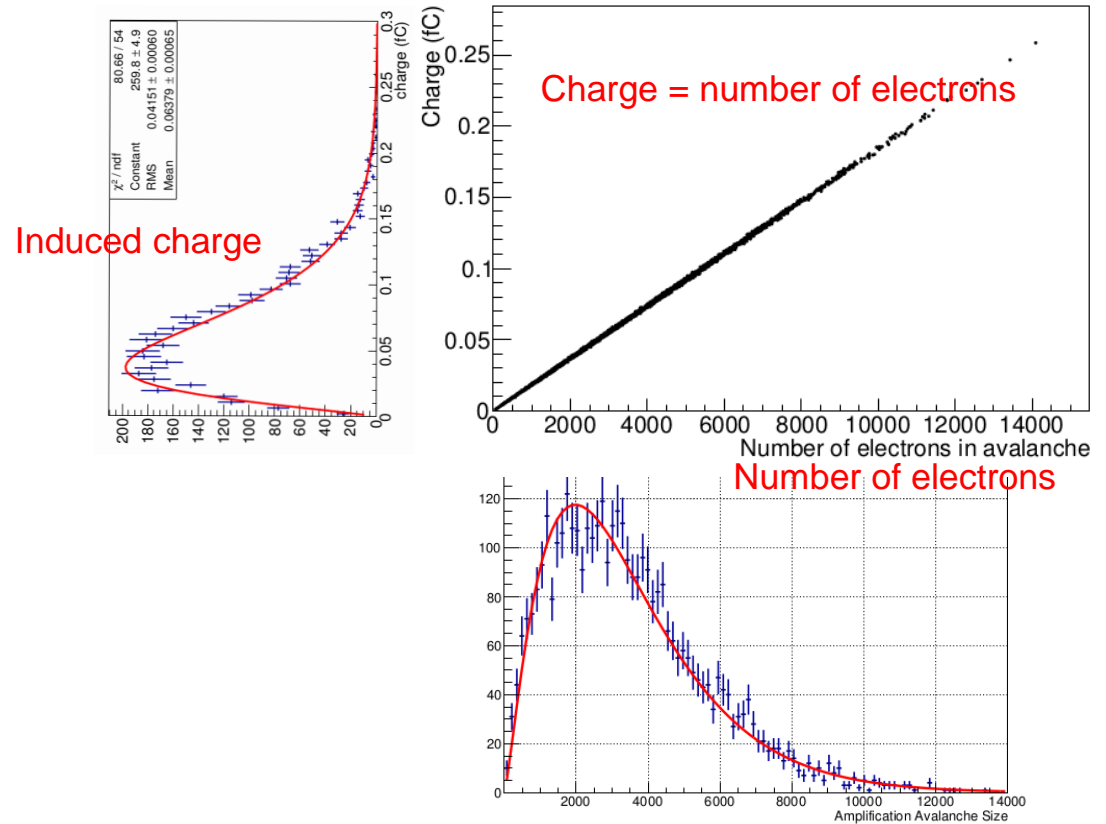
The distribution fit nicely with a Polya (red)
→ for each electron passing the mesh, we can get a representative number of electrons on the anode, by picking randomly from this Polya.

Detailed simulation with Garfield++ (4)

Stage 3 – Response of electronics

- Assume that the simulated pulse will be described with the difference of two logistics

- Find the parameters by using experimental data, in a statistically coherent way:
  a) Describe the pulse shape produced from one electron passing the mesh and entering the amplification region. Take distributions of "mean arrival times" for the electrons reaching the anode (from Garfield++) and convolute them with the shape of the electronic response, and
  b) Compare the result with the average waveform observed in the experimental data.

Anode
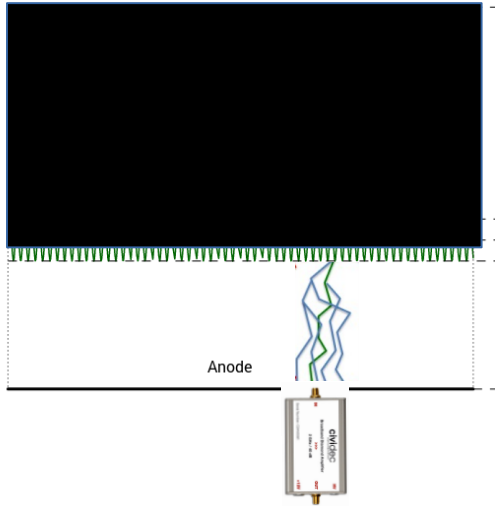
$$\frac{\langle S(t) \rangle_{Q_{tot}=Q}}{Q} = \int_0^\infty f(t-\tau) \, \langle \Phi(\tau) \rangle_{Q_{tot}=Q} \, d\tau$$

Normalized waveform

$$\frac{\text{Average waveform}}{\text{its total charge}} = \text{Response function of the electronics with all gains=1} \quad *^{(\text{convolution})} \quad \text{Distribution of Mean Arrival times}$$

(from the experimental data)

(from the simulation)
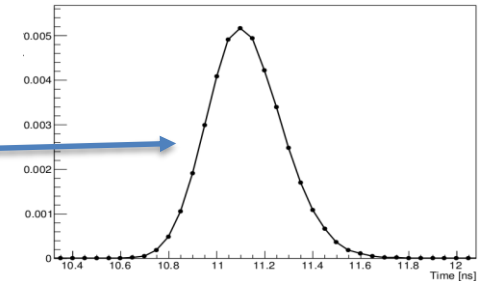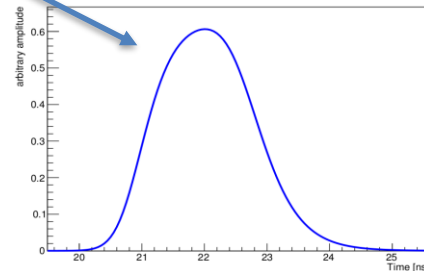
Detailed simulation with Garfield++ (5)

Pulse generation in Garfield++ –no extra electronic gain

N electrons pass through the mesh at times $\tau_1, \tau_2, \ldots, \tau_N$

Each one of these N electrons contributes a pulse **f(t)** (previous slide)**,
displaced by the respective time $\tau_1, \tau_2, \ldots, \tau_N$,**
where the size of the pulse is put as a random variable drawn from the
Polya describing the avalanche population (or the induced charge,
equivalently).

$$S(t) = \sum_{i=1}^{N} q_i \cdot f(t - \tau_i)$$

We thus, produce pulses with shapes like those in the experiment, but:

f(t-τ_i) is the shape of the electronics response: in order the simulated pulses to be exactly like
in the data, we need the Gain, G, of the electronics in order to construct **G*S(t)**

Pulse generation in Garfield++ – including electronic gain

G should be a constant. But**...**

Experiment
Simulation

450-375
G=30.2

450-400
G=27.8

450-425
G=21.9
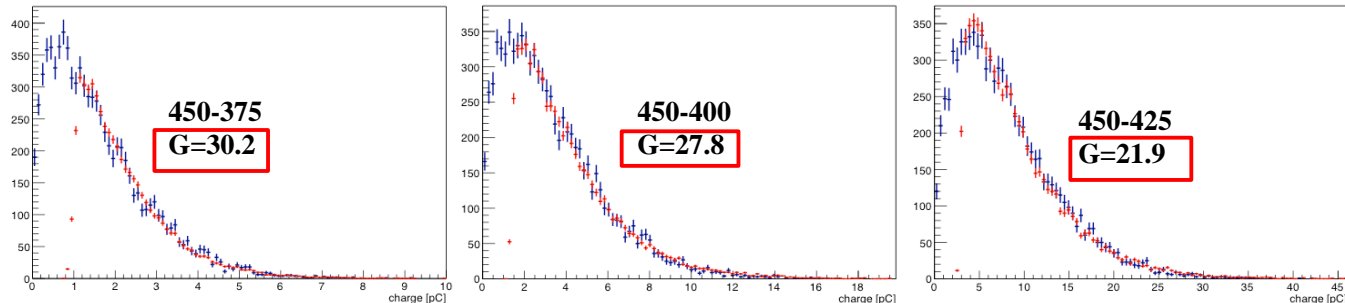
Detailed simulation with Garfield++ (6)

→ There must be another phenomenon not included here...

In Garfield++ , all interactions between electrons and molecules are included, but not between molecules themselves.

But Ne has excited states at high enough energies, that, when de-exciting, can cause the ionization of C_2H_6.

$$Ne^* + C_2H_6 \rightarrow Ne + C_2H_6^+ + e^-$$
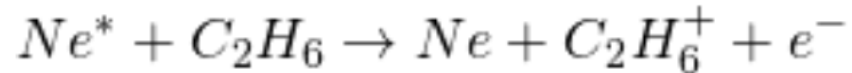
Such indirect ionizations are called the **"Penning effect"**

By putting as a free parameter, the probability, **r**, to have such an excited Ne to cause an ionization, we found that the value of **r=50%** for the **"Penning Transfer Rate"** allows to use a constant electronic gain G, independent of the voltage in the drift region.

29
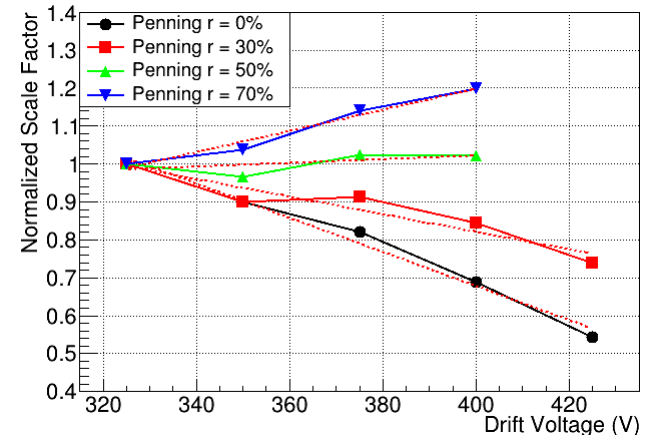
Detailed simulation with "trimmed" Garfield++

Black: Averaged PICOSEC waveforms in a certain e-peak charge region
Red: e-peak Simulation Prediction (Garfield++ and Electronics Response)
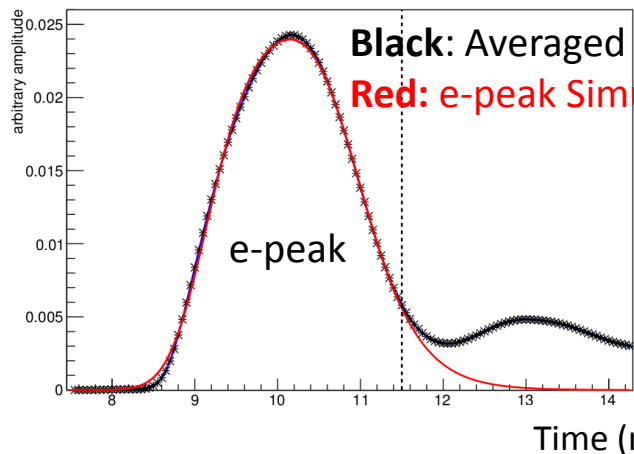
All behaviors seen in single p.e. laser data are also seen in these detailed Garfield++ simulations!!!

The Signal Arrival Time (SAT) depends non-trivially on the e-peak size:
* bigger pulses
  → smaller SAT
* higher drift field
  → smaller SAT

* Time resolution depends mostly on e-peak charge

SAT curves get to lower level as drift voltage increases

Different colors: different drift voltages
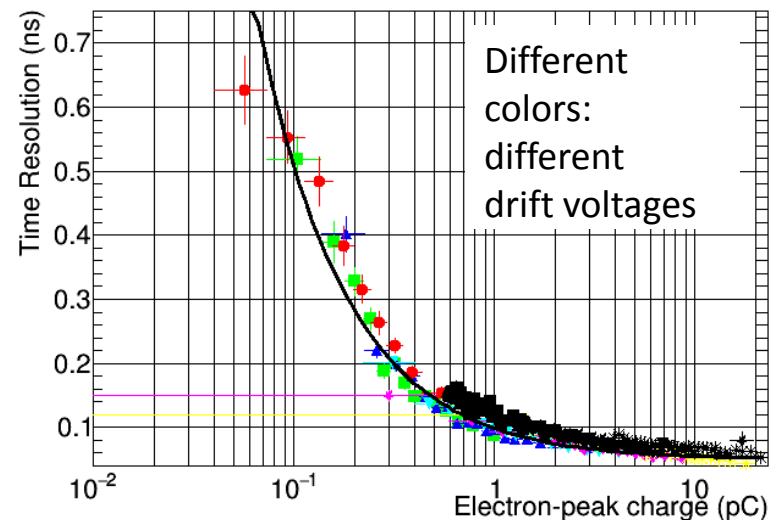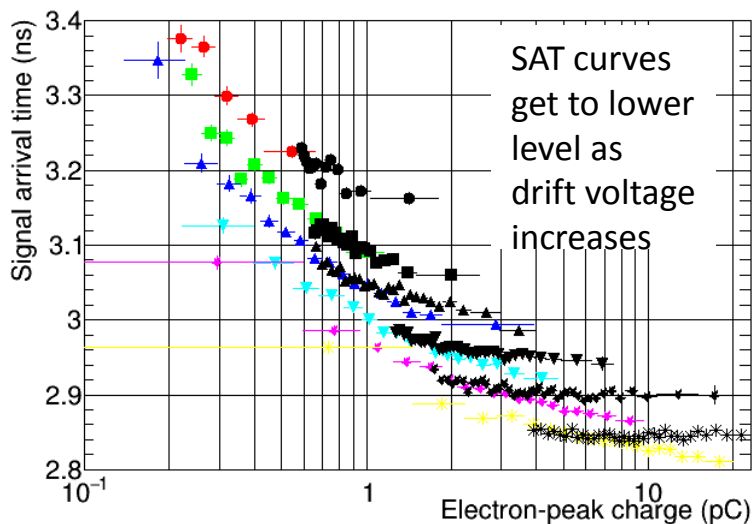
Color: Simulation – Black: Data

Detailed simulations: under the hood

d L

Pre-ionization track

D

Pre-amplification avalanche
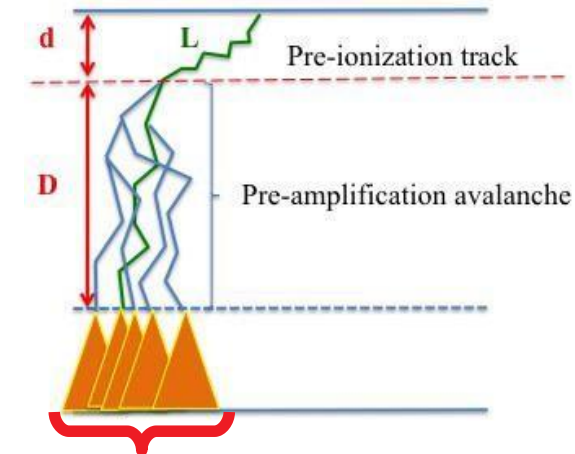
Gives e-peak pulse

Microscopic equivalent to e-peak's SAT = Mean Time (T) of all electron arrival times on the mesh
* **<SAT> linear with <T>**
* **RMS(SAT) linear with RMS(T)**

Correspondence of experimental Observables to Relevant Microscopic Variables
Sets of avalanches of a certain e-peak charge

χ^2 / ndf 12.16 / 113
Constant 0.0004358 ± 0.001932
Slope 0.02575 ± 4.36e−05

Mean e-peak charge [pC]

Number of electrons passing through mesh

χ^2 / ndf 96.91 / 113
Constant 1.675 ± 0.01694
Slope 1.023 ± 0.01359

Mean SAT [ns]

Mean electron arrival time [ns]

χ^2 / ndf 49.53 / 113
Constant −0.0009093 ± 0.001344
Slope 1.017 ± 0.01768

RMS SAT [ns]

RMS electron arrival time [ns]

Detailed simulations: under the hood

d L

Pre-ionization track

D

Pre-amplification avalanche

Gives e-peak pulse

Total arrival time reduces with avalanche length

Time (ns)

1.2

1

0.8

0.6

0.4

0.2

0

Total Time

Pre—Ionization Time

Avalanche Time

Sum of the 1st Electron and Avalanche Times

0 20 40 60 80 100 120 140 160 180

drift/anode:
-425V / +450 V

154 µm/ns

134 µm/ns

Avalanche length, D (µm)

Avalanche runs with higher drift velocity than **pre-ionization electron**

So, SAT "slewing" seen in single p.e data is explained:

SAT reduces with avalanche length

Long avalanches → big e-peak charge } **SAT reduces with e-peak charge** **!**

More counter-intuitive observations found related to collective, emerging properties of the avalanche!!

Let us be inspired by the phenomenon of "Quenching"

From Rob Veenhof

Electrons in Ar/CO_2 at E=1 kV/cm

Elastic scatterings WITHOUT any significant energy loss
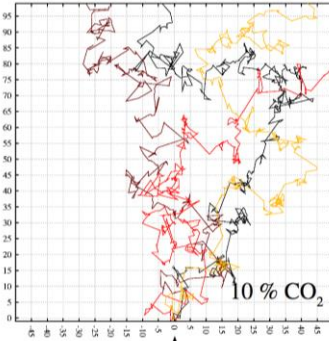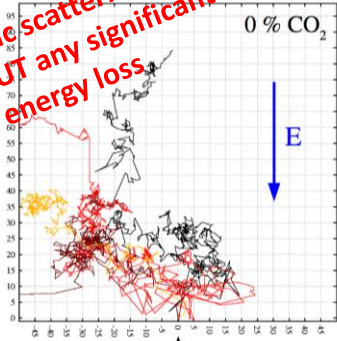
Scatterings WITH significant energy loss
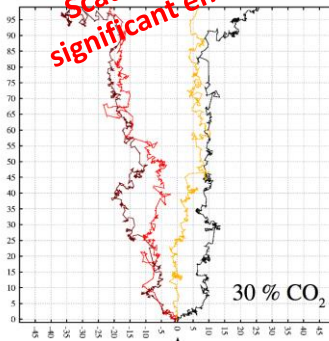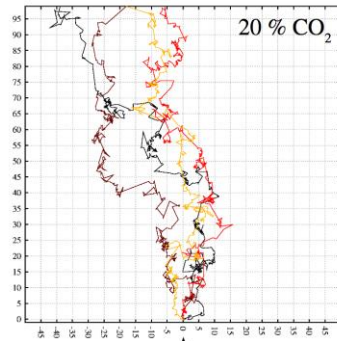
In the case of "quenching", the energy loss results in higher drift velocity !!!

Let us be inspired by the phenomenon of "Quenching"

From Rob Veenhof

Electrons in Ar/CO_2 at E=1 kV/cm

Elastic scatterings WITHOUT any significant energy loss
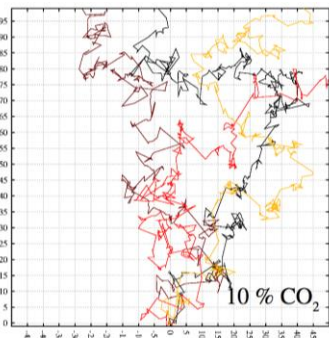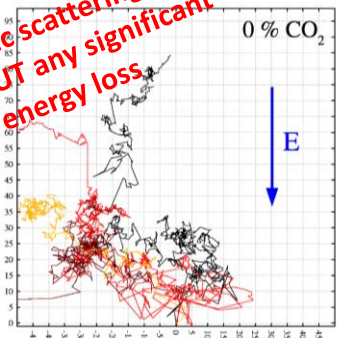
Scatterings WITH significant energy loss
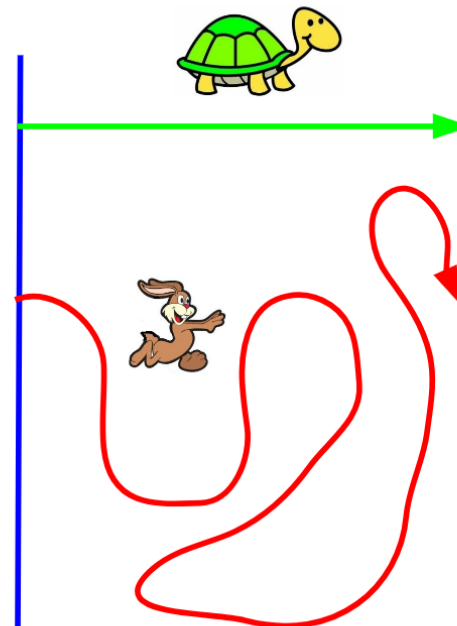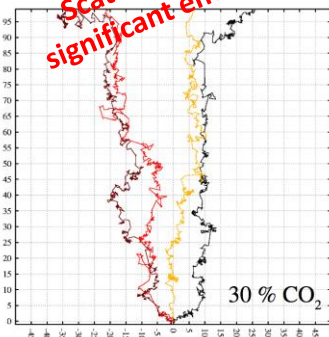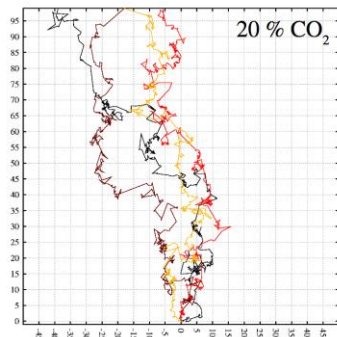
In the case of "quenching", the energy loss results in higher drift velocity !!!

Phenomenological model: A deeper looking under the hood

- An ionizing electron in the avalanche, every time it ionizes, will gain a time ξ_i relative to an electron that undergoes elastic scatterings only.
- A new produced electron by ionization starts with low energy, suffers less delay due to elastic backscattering compared to its parent. Relative to his parent it will have a time-gain ρ_i
- Parameters ξ_i and ρ_i should follow a joint probability distribution determined by the physical process of ionization and the respective properties of interacting molecules

  - The collective effect of time-gains ξ_i, is a change in drift velocity from V_p, which is the photoelectron drift velocity before ionization, to an effective drift velocity V_{ea}, which is the drift velocity of an ionizing electron in the avalanche. By taking V_{ea} to be the drift velocity of any electron in the avalanche, the energy-loss effect on the drift of the parent has been taken into account.
  - When a new electron is produced in the avalanche, through ionization, it will gain time ρ_i, at its production, which is assumed to follow a distribution with mean value ρ and variance w^2. From that moment onwards, this new electron propagates with drift velocity V_{ea} as any other existing electron in the avalanche.

35
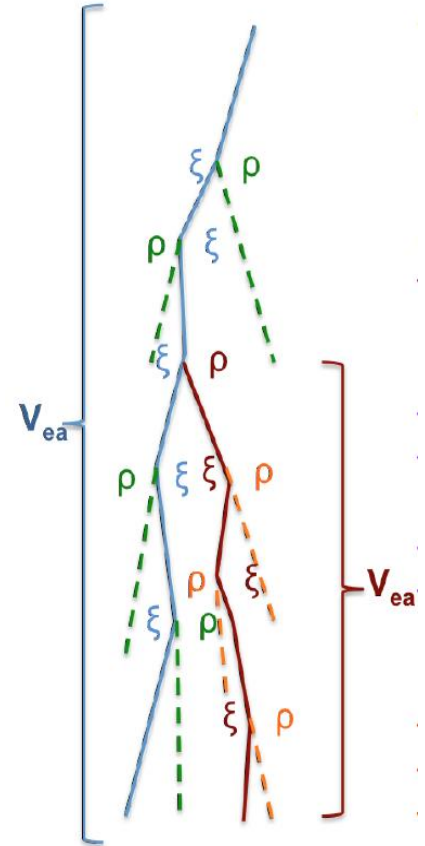
Understood in terms of phenomenological model
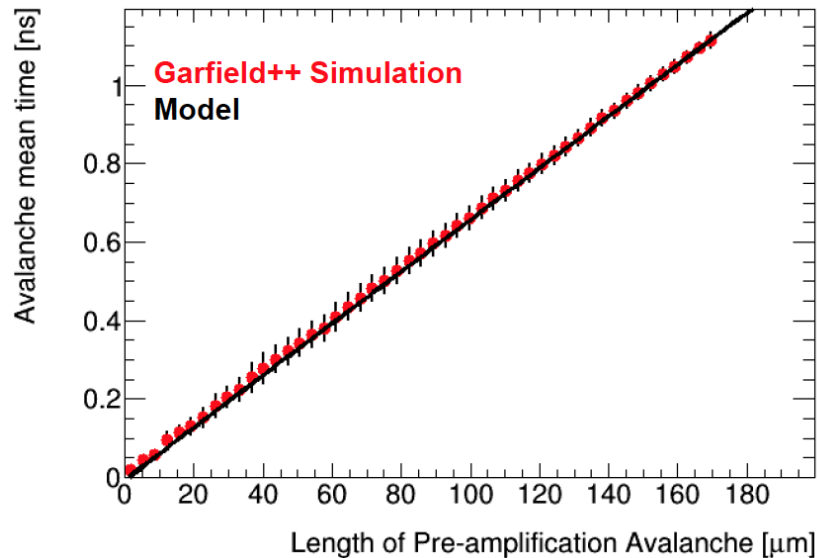
We can predict the effective drift velocity of the avalanche
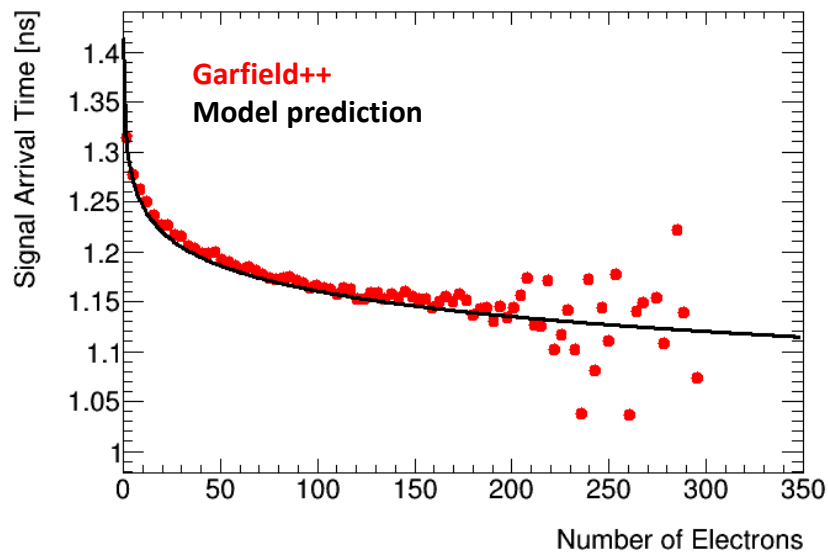
We can describe and explain the SAT dependence on the number of avalanche's electrons (i.e. on the e-peak size)

- The other parameters of the model are: the drift velocity of the photoelectron and the first Townsend coefficient.
- The model treats the number of electrons in an avalanche as continue variable.

Understood in terms of phenomenological model(2)

We can describe and explain the Resolution dependence on the length of the avalanche and on the number of avalanche's electrons (i.e. on the e-peak size)

Garfield++
Model prediction

drift/anode:
-425V / +450V

Lines are not fits: they are model predictions!

drift/anode:
-425V / +450V

total

p.e. contribution

avalanche contribution
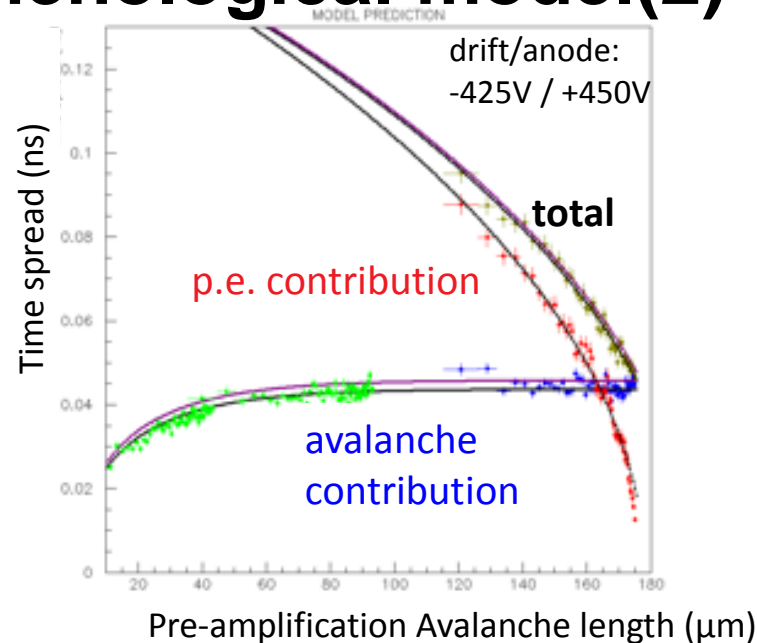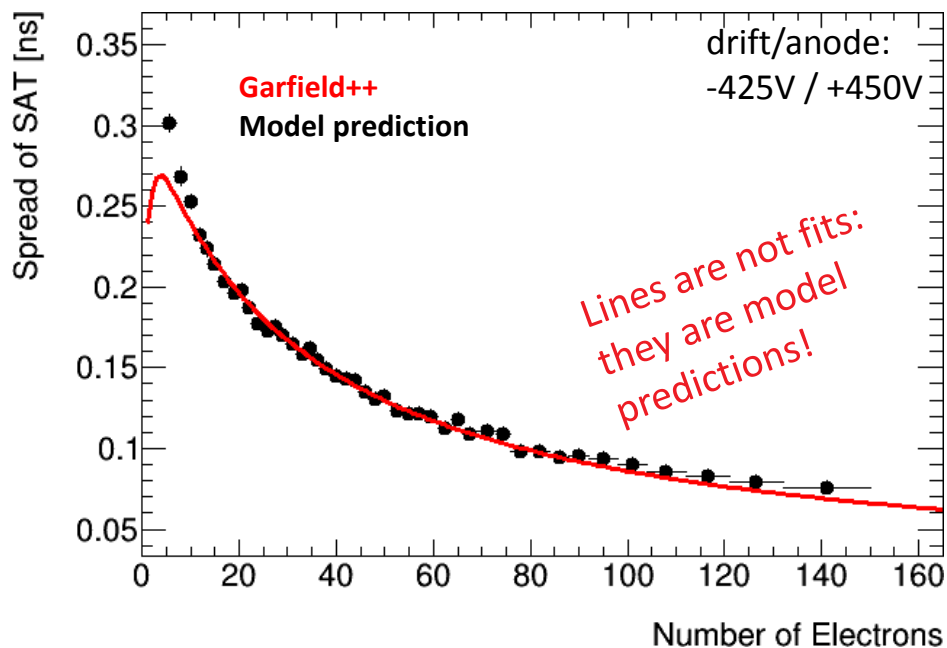
The model describes SAT and Resolution
a) vs. avalanche length &
b) vs. number of electrons in avalanche
          (i.e, vs. e-peak charge)
→ Before and after the mesh
Not only averages and RMS, but full distributions, vs. values of operational parameters (e.g., drift voltage)   arXiv:1901.10779v1 [physics.ins-det]

!

3. Estimation of the No of pes per MIP

A consistent and unbiased procedure to estimate the number of photoelectrons per MIP(1)

Precise alignment based on the charge-weighted beam profile
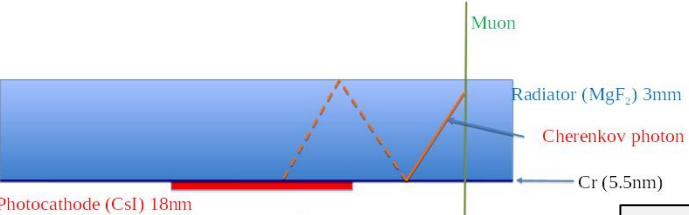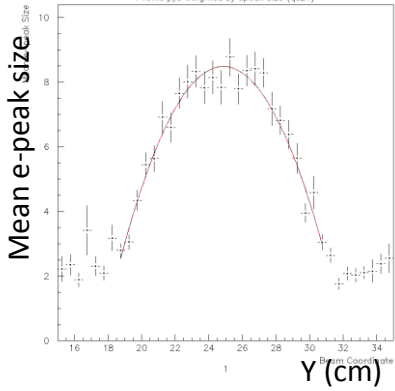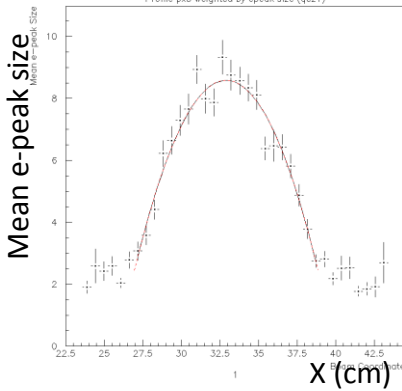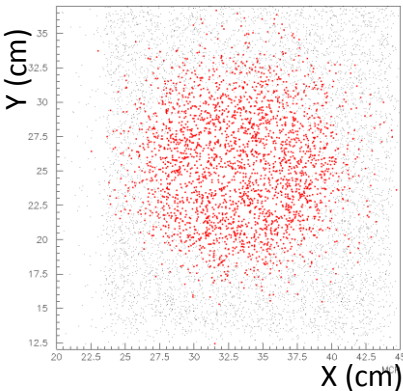
Determination of the anode geometrical acceptance taking into account reflections

Refl: 22%
Abs: 20%
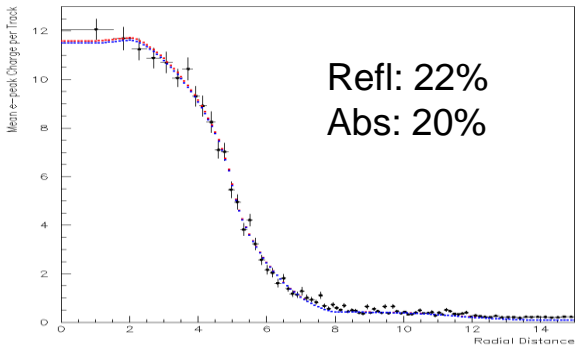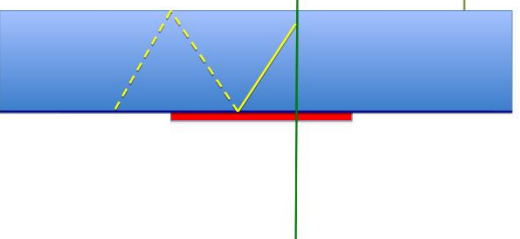
Mean charge per track (pC) vs the track radial distance (mm)

A consistent and unbiased procedure to estimate the number of photoelectrons per MIP(2)

Determination of the charge distribution parameters when the PICOSEC **MM responds to a single-pe** using UV calibration data
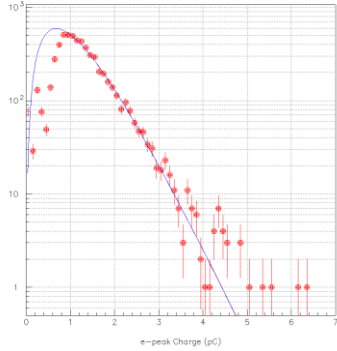
A Polya fit to the single-pe charge distribution

$$P_{spe}\left(Q; a=b=\theta+1, \overline{Q}_e\right)dQ = \frac{1}{Q_e}\frac{(\theta+1)^{(\theta+1)}\left(Q/\overline{Q}_e\right)^{\theta}}{\Gamma(\theta+1)}e^{-(\theta+1)Q/\overline{Q}_e}dQ$$

$$E\left[Q_{spe}\right] = \overline{Q}_e = \langle Q_e \rangle$$

$$V\left[Q_{spe}\right] = \frac{1}{\theta+1}\langle Q_e \rangle^2 = RMS^2$$

RMS	Mean
0.6433	1.0668
0.6498	1.1102
0.6452	1.117
0.6388	1.0786
0.6398	1.028
0.64305	1.0118

Take into account systematic errors due to threshold effects

Fit the charge distribution of the PICOSEC **response to muons**

If N is the mean number of pes produced per muon track, then a muon passing through the radiator at distance R from the anode center will result to a PICOSEC signal with charge Q.
Q follows a p.d.f. F(Q,R;N) which can be expressed using the geometrical acceptance A(R), as a convolution of a Poissonian distribution with mean N·A(R)

$$\Pi(N_{pe}; N, A(R)) = \frac{[N \cdot A(R)]^{N_{pe}}}{N_{pe}!} \cdot \exp[-N \cdot A(R)]$$

and the multi-Polya distribution

$$P(Q; N_{pe}, \theta, \overline{Q}_e) = \underbrace{P_{spe} \otimes P_{spe} \cdots \otimes P_{spe}}_{N_{pe}\ times} = \frac{1}{Q_e}\frac{(\theta+1)^{N_{pe}(\theta+1)}(Q/\overline{Q}_e)^{N_{pe}(\theta+1)-1}}{\Gamma(N_{pe}(\theta+1))} \cdot \exp[-(\theta+1) \cdot Q/\overline{Q}_e]$$

as

$$F(Q,R;N) = \sum_{N_{pe}=0}^{\infty} \Pi(N_{pe}; N, A(R)) \cdot P(Q; N_{pe}, \theta, \overline{Q}_e)$$

A consistent and unbiased procedure to estimate the number of photoelectrons per MIP(3)

CsI Photocathode
All Tracks within 6mm from Center

Red line: Fitted curve
Black dots: Data

Inner Tracks within 3.5mm from Center
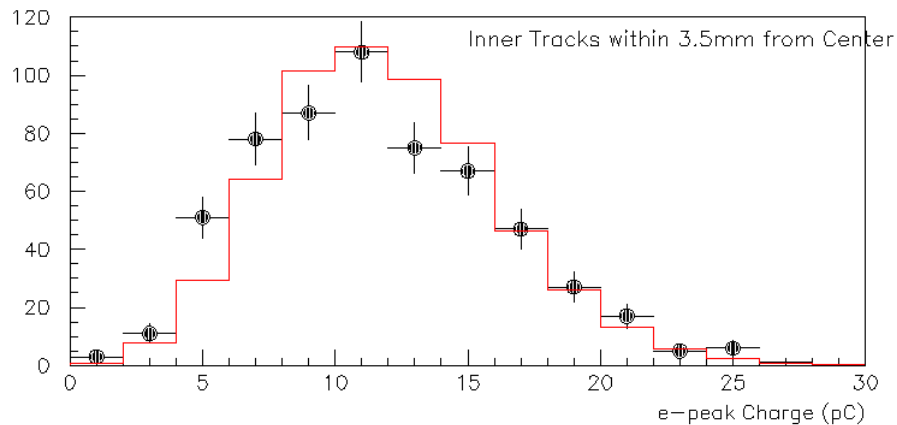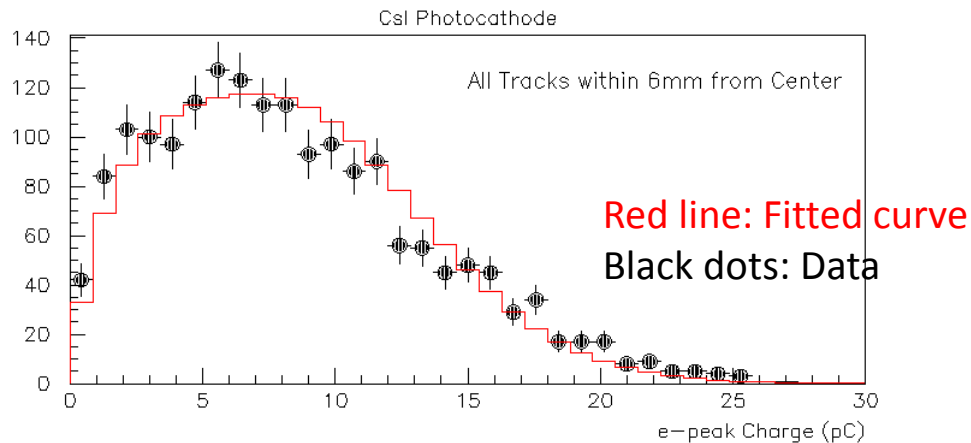
11.5 ±0.4(stat)±0.5(syst) photoelectrons per muon track

Resolution Prediction Assuming 1/sqrt(Npe) Dependence

Normalized to the 1st Data Point

Fit for Normalization

Line: Prediction
Black dots: Data
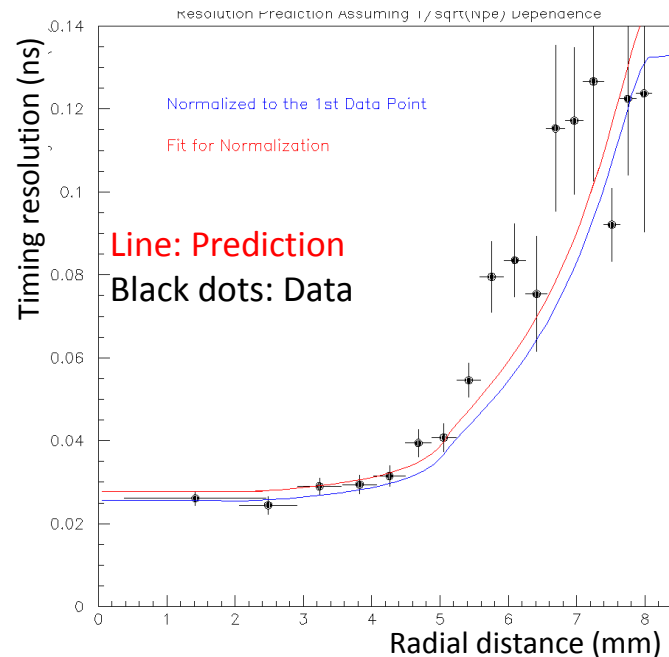
Resolution prediction vs distance from the anode center, assuming **1/sqrt(Npe)** dependence

4. Towards a robust, large-scale detector

Detector stability

Photocathode robustness

Large area coverage

Detector stability – Resistive Micromegas

Best resolution was at voltages which give high currents on anode: **robust anode**

Resistive strips (MAMMA)
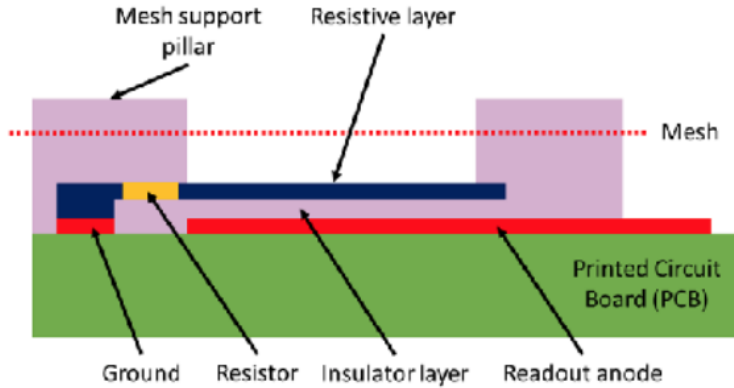
Readout beneath resistive layer: picks up signal from above

Floating strips (COMPASS)
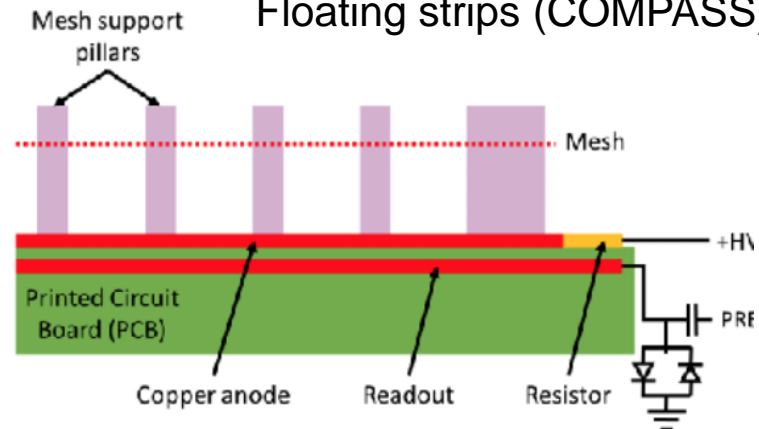
Copper Layer to HV via resistor; Readout "floating"

Resistive readouts operate stably at high gain in neutron fluxes of 10^6 Hz/cm^2.

T. Alexopoulos et al., NIMA 640 (2011) 110-118.

Non resistive ← MAMMA results → With resistive strip

discharges

~ no discharges
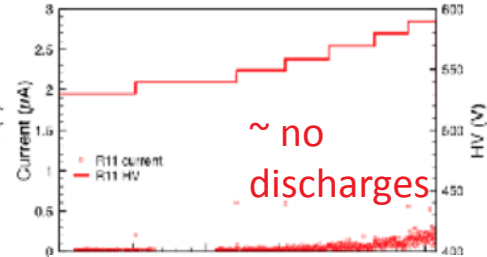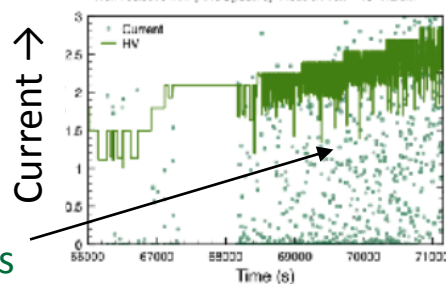
Detector stability – Resistive Micromegas

Beam results with protected anodes
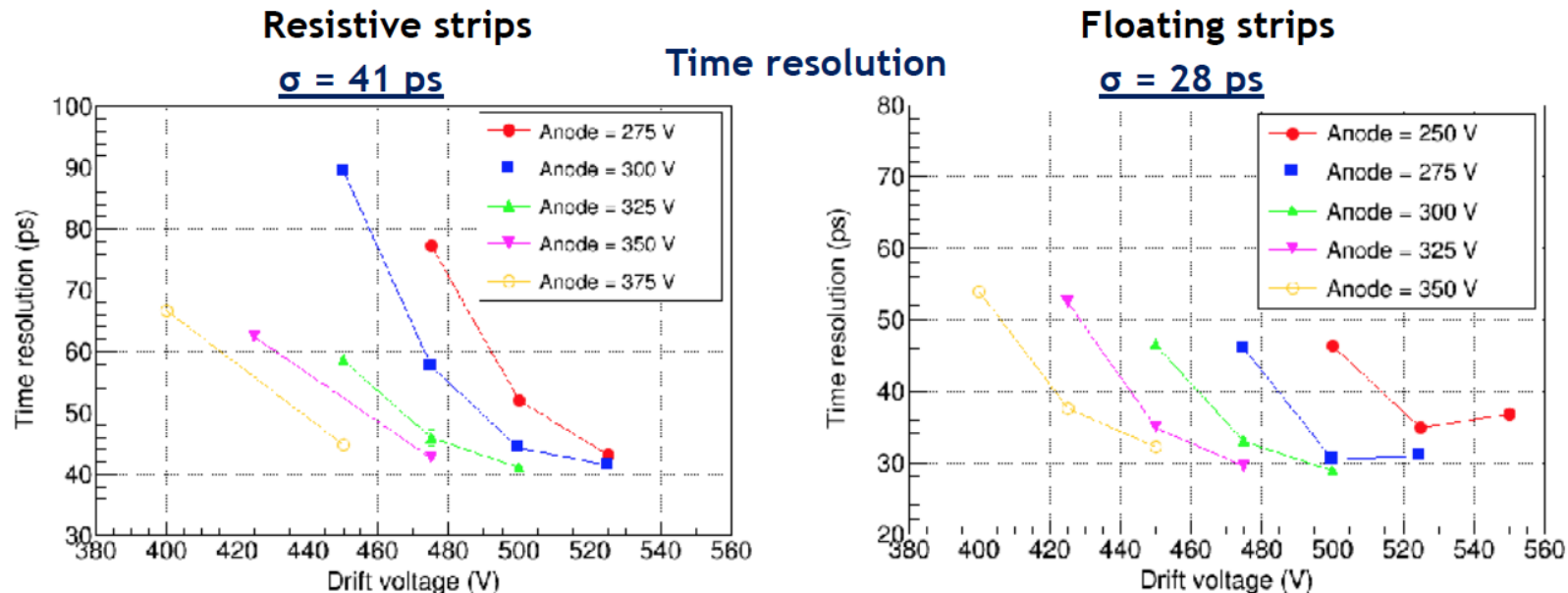
- Values not far from the Picosec bulk readout.
  - **Resistive strips:** <u>41 ps</u> (10 MΩ/□), <u>35 ps</u> (300 kΩ/□).
  - **Floating strips:** <u>28 ps</u> (25 MΩ).
- Resistive readouts worked during hours in intense pion beam.

Photocathode robustness – Problems with CsI

CsI sensitive to humidity, ion backflow and sparks
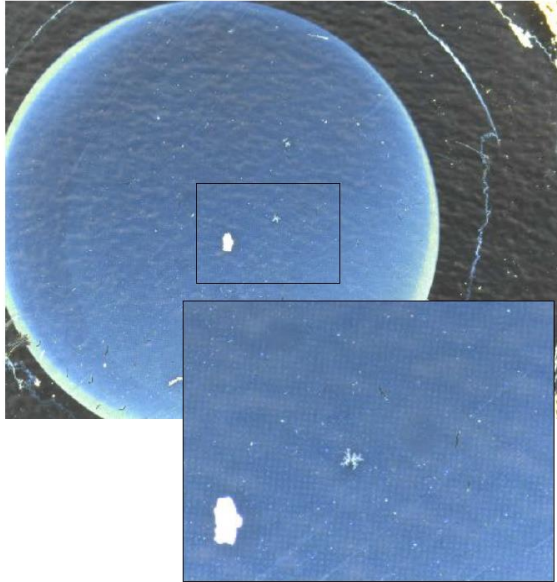
Ion backflow on CsI
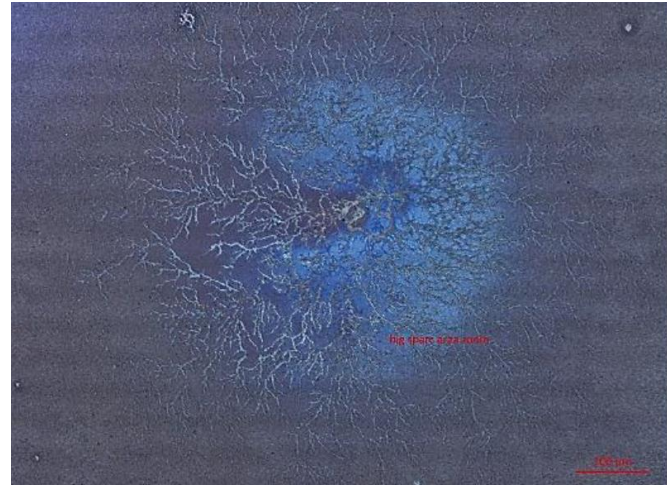
CsI photocathode after spark

Photocathode robustness – Protection and alternatives

Photocathode robustness preserves QE and thus detector efficiency
and timing resolution during long-period operation

- **Protection layers on CsI** and **alternative photocathode materials** (Metallic, DLC, B_4C, nano diamond powder, CVD diamond) were tested

- For each material, the working point with the best time resolution has to be determined

- Inherently robust materials, but with lower QE

Most promising performance results for non-CsI are from **Diamond-Like Carbon (DLC)**, which also seems robust:
- atmospheric conditions for a few months
- irradiated with pions, in a resistive MM prototype →minimal reduction of Npe/MIP

3mm MgF_2 + DLC of different thicknesses:

Photocathode robustness – Diamond-like Carbon

- 2.5 nm DLC time resolution up to 34 ps observed
- Results repeatable in independent samples and measurements
- Additional tests with heating treatment under N_2 and H_2
- Additional ageing tests under pions
- Samples survived rough transport from China

Thickness of DLC film (nm)	Npe/per muon	Detection efficiency for muons
1	Bad	Bad
2.5	3.7	97%
5	3.4	94%
7.5	2.2	70%
10	1.7	68%
5 nm Cr + 18 nm CsI	7.4	100%

PRELIMINARY

2.5 nm DLC in Bulk MM

A/D Voltage	Time Res. (ps)
250/550	37
250/575	34
275/525	38
275/550	34
300/500	39
300/525	34

Large-area coverage - Multi-pad MicroMegas
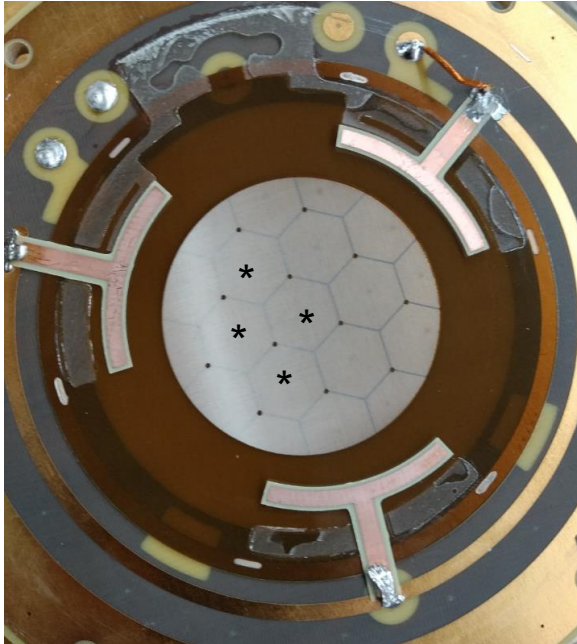
- **Like the single-pad (MgF$_2$/CsI/bulkMM/COMPASS gas) PICOSEC which achieved 24ps per MIP**

- Hexagonal pads 5mm side
- Readout 4 pads → 2 oscilloscopes

Large-area coverage - Multi-pad MicroMegas

Multi-pad: individual pad response vs. R

- Study response vs. R : distance of track impact from pad center

  - 0<R<2mm: full Cherenkov cone (3mm) inside pad
  - 2 < R < 4.33mm: Cherenkov cone (3mm) mostly inside pad
  - 4.33 < R < 7.5mm: Cherenkov cone (3mm) mostly outside pad

Hexagonal pads 5mm side

0. < R < 2. mm
2. < R < 4.33 mm
4.33 < R < 7.5 mm

SAT (ns)

e-peak charge (pC)

0. < R < 2. mm
2. < R < 4.33 mm
4.33 < R < 7.5 mm

Time Resolution (ns)

<20ps for large e-peaks

PRELIMINARY
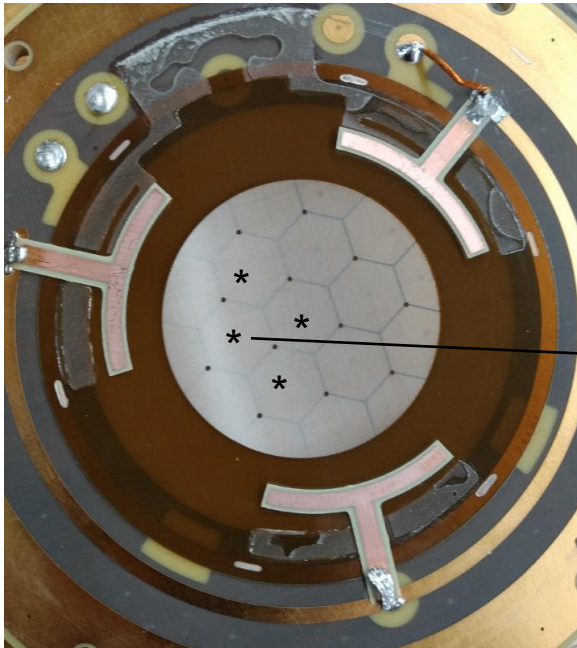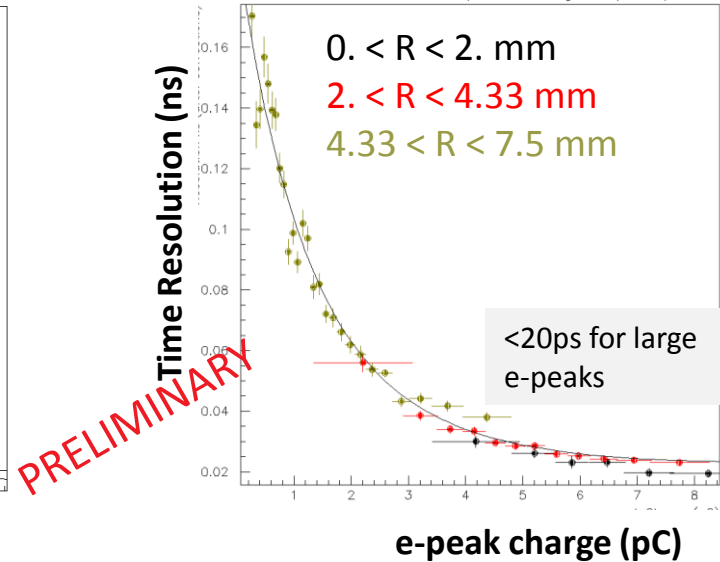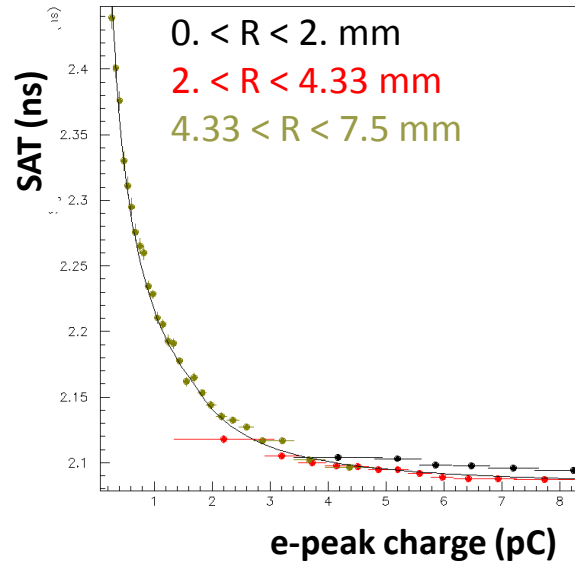
e-peak charge (pC)

e-peak charge should have all info about where is Cherenkov cone compared to pad. Indeed, universal curves vs. e-peak charge:

Large-area coverage - Multi-pad MicroMegas

Multi-pad: Same resolution as single-pad

At center of each pad (0<R<2mm):

Timing resolution of **25ps for all pads**
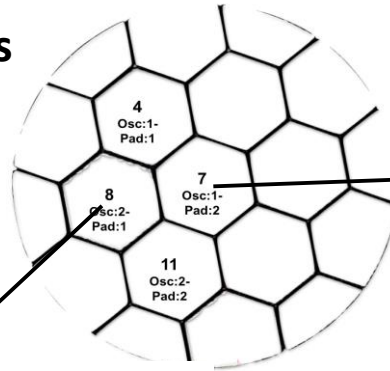
Individual pad response

σ_{tot}=25ps

χ^2/ndf 57.44	/	56
P1	101.9 ±	27.03
P2	0.7209E-03 ±	0.8397E-03
P3	0.2892E-01 ±	0.1951E-02
P4	68.56 ±	24.39
P5	0.1960E-02 ±	0.1523E-02
P6	0.1449E-01 ±	0.3714E-02

PRELIMINARY

ΔT = Time after all corrections (ns)

Individual pad response

σ_{tot}=25ps

χ^2/ndf 35.43	/	41
P1	4.241 ±	8.401
P2	-0.7759E-02 ±	0.2665E-01
P3	0.9064E-01 ±	0.1415
P4	152.7 ±	5.465
P5	0.6543E-02 ±	0.7831E-03
P6	0.2296E-01 ±	0.2143E-02

PRELIMINARY

ΔT = Time after all corrections (ns)
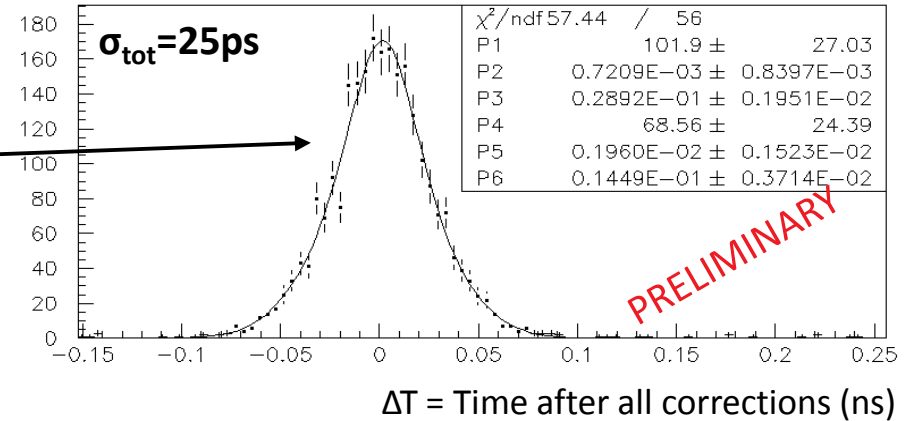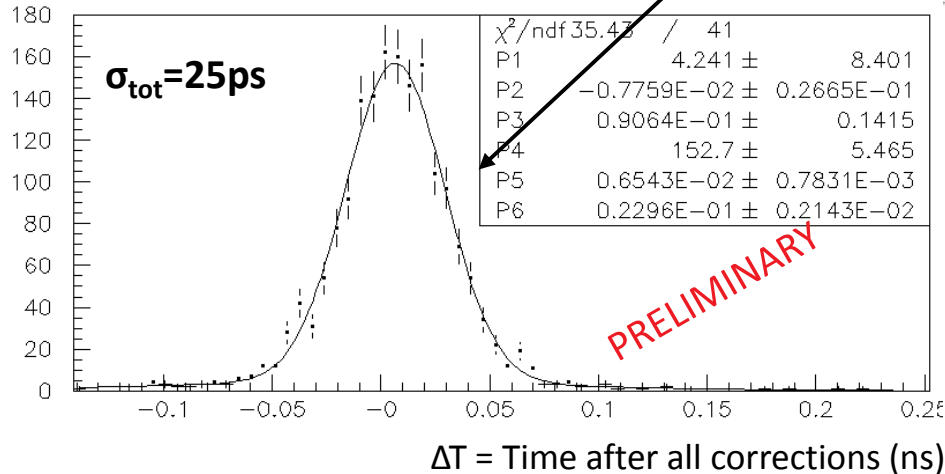
Large-area coverage - Multi-pad MicroMegas

Individual pad responses for tracks falling around the "three-pads" region

These are not the easiest regions

Pillars of ~650µm diameter

200µm inter-pad space

Individual pad responses

σ= 86 ps

χ^2/ndf 38.58	/ 44	
P1	12.11 ±	15.41
P2	−0.2725E−01 ±	0.2160E−01
P3	0.1436 ±	0.7168E−01
P4	83.45 ±	9.678
P5	0.3485E−02 ±	0.3794E−01
P6	0.5247E−01 ±	0.1128E−01

ΔT = Time after all corrections (ns)

PRELIMINARY

σ= 70 ps

χ^2/ndf 38.75	/ 39	
P1	27.65 ±	6.065
P2	−0.1345E−01 ±	0.5085E−02
P3	0.8745E−01 ±	0.6801E−02
P4	75.02 ±	6.929
P5	0.6353E−02 ±	0.2367E−02
P6	0.3238E−01 ±	0.3194E−02

ΔT = Time after all corrections (ns)

σ= 81 ps

χ^2/ndf 43.88	/ 38	
P1	22.38 ±	4.475
P2	−0.3830E−01 ±	0.8286E−02
P3	0.1134 ±	0.9807E−02
P4	86.41 ±	6.122
P5	0.1191E−01 ±	0.2392E−02
P6	−0.3683E−01 ±	0.3582E−02

ΔT = Time after all corrections (ns)

Large-area coverage - Multi-pad MicroMegas

Combining pads for tracks falling around the "three-pads" region

Individual pad responses
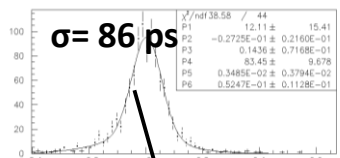
σ= 86 ps

ΔT = Time after all corrections (ns)

σ= 81 ps

ΔT = Time after all corrections (ns)

σ= 70 ps
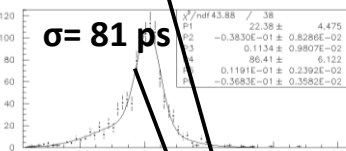
ΔT = Time after all corrections (ns)

Combining pads event-by-event

4
Osc:1-
Pad:1

8
Osc:2-
Pad:1

7
Osc:1-
Pad:2

11
Osc:2-
Pad:2

$$\chi^2 = \sum_{i=1,3} \frac{\left(\left[t_i - \left\{\langle SAT\rangle(R_i,\theta_i) - \langle SAT\rangle(R_i,90^o)\right\} - \left\{SL(Q)\right\} - \hat{t}\right]\right)^2}{\left(\operatorname{Re} s(Q_i)\right)^2}$$

σ= 31 ps

ΔT = Time after all corrections (ns)

ΔT / σ_t
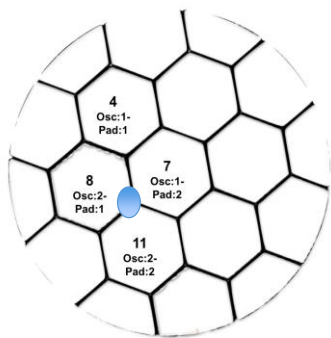
Naive estimation:
<σ>/sqrt(3)≈45 ps
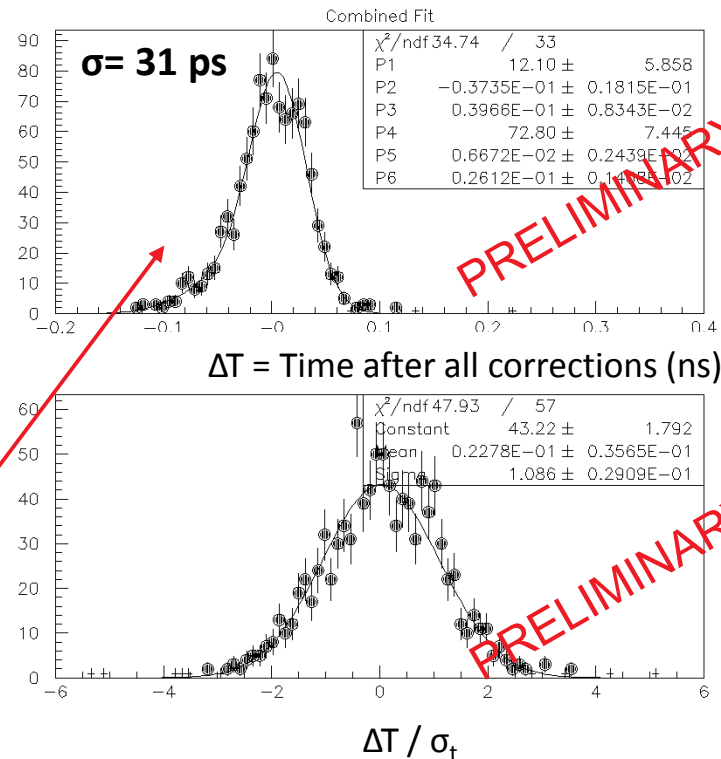
Similar results all across the area covered by the 4 pads

PRELIMINARY

52

Large-area coverage

Several variants of multi-channel PICOSEC prototypes in development / under test, associated with scaling to larger areas:

- Signal routing and sharing across pads
- Multi-channel amplifiers and digitizers
- Resistive multi-pad anode
- Detector uniformity
- Large Cherenkov radiators
- Mechanics to preserve precise gaps
- Compact detector vessel
- …
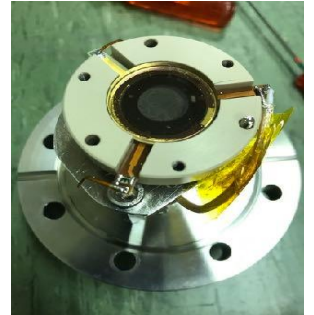
Single pad ø 1cm
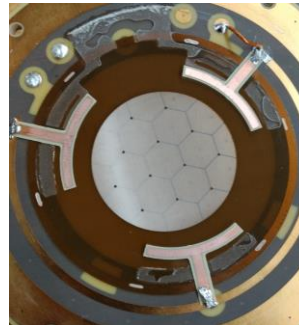
Multi-pad ⬡ 1cm
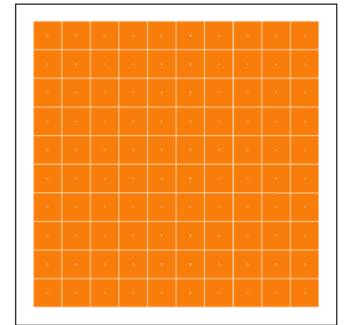
10 x 10 module

Conclusions

- **PICOSEC MicroMegas: a detector with precise timing:**

  – Single-channel prototype in Laser and Particle beams

  – 76ps for single photoelectrons, 24ps resolution for timing MIPs

- **A well-understood detector:**

  – reproduce observed behavior with detailed simulations and a phenomenological model: valuable tool for parameter-space exploration

- **Efficient photocathode**

  – consistent and unbiased procedure to estimate the number of photoelectrons per MIP

- **Towards a large-scale detector: multi-channel, robustness, photocathodes**

  – response of multi-channel PICOSEC prototype: similar precision as the single-channel prototype, for any impact point of a MIP, progress towards a robust detector

Thank you

Stage 3 – Electronics (2) – technique is consistent and unibiased

$\bar{S}(t)$

$$P_{Q_{tot}=Q}(\tau_1, ..., \tau_k, q_1, ..., q_k; k) =$$

$$= \frac{\delta\left(Q - \sum_{i=1}^{k} q_i\right) \cdot R(k) \cdot \prod_{i=1}^{k} \Phi(\tau_i; k) \cdot \prod_{i=1}^{k} G(q_i)}{N(k)}$$

where

$$N(k) = \int_0^\infty \cdots \int_0^\infty \delta\left(Q - \sum_{i=1}^{k} q_i\right) \cdot R(k) \cdot \prod_{i=1}^{k} G(q_i) dq_1...dq_k$$

$$\langle S(t)\rangle_{Q_{tot}=Q} =$$

$$= \sum_{k=1}^\infty R(k) \int_0^\infty \cdots \int_0^\infty \sum_{i=1}^{k} q_i f(t - \tau_i) \cdot \delta\left(Q - \sum_{i=1}^{k} q_i\right) \cdot$$

$$\cdot \prod_{j=1}^{k} \Phi(\tau_j; k) \cdot \prod_{j=1}^{k} G(q_j) dq_1...dq_k d\tau_1...d\tau_k$$

$$\langle S(t)\rangle_{Q_{tot}=Q} = \sum_{k=1}^\infty R(k) \sum_{i=1}^{k} \int_0^\infty f(t - \tau_i)\Phi(\tau_i; k)d\tau_i \cdot$$

$$\cdot \int_0^\infty \cdots \int_0^\infty q_i \cdot \delta\left(Q - \sum_{i=1}^{k} q_i\right) \cdot \prod_{j=1}^{k} G(q_i) dq_1...dq_k$$

$$\langle q_i\rangle_{Q=\sum_{j=1}^{k} q_j} = \frac{\int_0^\infty \cdots \int_0^\infty q_i \cdot \delta\left(Q - \sum_{i=1}^{k} q_i\right) \cdot \prod_{j=1}^{k} G(q_i) dq_1...dq_k}{N(k)}$$

$$\langle S(t)\rangle_{Q_{tot}=Q} = \sum_{k=1}^\infty R(k)N(k) \sum_{i=1}^{k} \int_0^\infty f(t - \tau_i)\Phi(\tau_i; k)d\tau_i \cdot$$

$$\cdot \int_0^\infty \cdots \int_0^\infty \frac{q_i \cdot \delta\left(Q - \sum_{i=1}^{k} q_i\right) \cdot \prod_{j=1}^{k} G(q_i)}{N(k)} dq_1...dq_k$$

$$\langle S(t)\rangle_{Q_{tot}=Q} = \sum_{k=1}^\infty R(k)N(k) \cdot \sum_{i=1}^{k} \langle q_i\rangle_{Q=\sum_{j=1}^{k} q_j} \int_0^\infty f(t-\tau_i)\Phi(\tau_i; k)d\tau_i$$

$$\int_0^\infty f(t - \tau_i)\Phi(\tau_i; k)d\tau_i = \int_0^\infty f(t - \tau)\Phi(\tau; k)d\tau$$

$$\langle S(t)\rangle_{Q_{tot}=Q} = \sum_{k=1}^\infty R(k)N(k) \int_0^\infty f(t - \tau)\Phi(\tau; k)d\tau \sum_{i=1}^{k} \langle q_i\rangle_{Q=\sum_{j=1}^{k} q_j}$$

$$= Q\sum_{k=1}^\infty R(k)N(k) \int_0^\infty f(t - \tau)\Phi(\tau; k)d\tau$$

$$= Q\int_0^\infty f(t - \tau) \left\{\sum_{k=1}^\infty R(k)N(k)\Phi(\tau; k)\right\} d\tau$$

$$\langle \Phi(\tau)\rangle_{Q_{tot}=Q} = \sum_{k=1}^\infty R(k)N(k)\Phi(\tau; k)$$

Understood in terms of phenomenological model

- Known in literature that quenchers in the gas-mix increase drift velocity →

- **Model**: assume a time-gain per inelastic interaction compared to elastic interactions

Electron population on the mesh→

Electron polulation on the mesh→

Electron population on the mesh
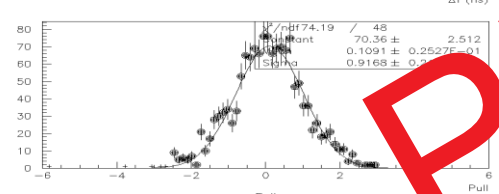
Multi- pad: Tracks are selected within a circle of 1.5 mm radious

μ=1.6 ± 2ps
σ= 25± 1.5 ps

μ=0 ± 2ps
σ= 31± 1.5 ps

μ=2 ± 2ps
σ= 31± 1.5 ps

μ=5 ± 2ps
σ= 25± 1.5 ps

Multi- pad: Tracks are selected within a circle of 1.5 mm radious

μ=1.6 ± 2ps
σ= 25± 1.5 ps

μ=-2 ± 2ps
σ= 29± 1.5 ps

μ=-4 ± 2ps
σ= 32± 1.5 ps

μ=-1.5 ± 2ps
σ= 33± 1.5 ps

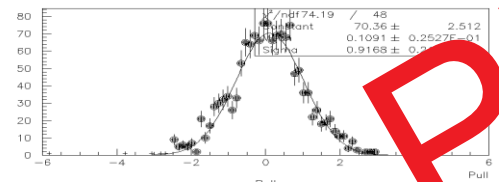# Multi- pad: Tracks are selected within a circle of 1.5 mm radious

μ=1.6 ± 2ps
σ= 25± 1.5 ps

μ= 3 ± 2ps
σ= 32 ± 1.5 ps

μ= 1 ± 2ps
σ= 33± 1.5 ps

μ= 4 ± 2ps
σ= 31± 1.5 ps

PRELIMINARY